Circulation Research
JOURNAL OF THE AMERICAN HEART ASSOCIATION

A Novel Mouse Model of Atherosclerotic Plaque Instability for Drug Testing and Mechanistic/Therapeutic Discoveries Using Gene and MicroRNA Expression Profiling

Yung-Chih Chen, Anh Viet Bui, Jeannine Diesch, Richard Manasseh, Christian Hausding, Jennifer Rivera, Izhak Haviv, Alex Agrotis, Nay Min Htun, Jeremy Jowett, Christoph Eugen Hagemeyer, Ross D. Hannan, Alex Bobik and Karlheinz Peter

Circ Res. 2013;113:252-265; originally published online June 7, 2013;
doi: 10.1161/CIRCRESAHA.113.301562
Circulation Research is published by the American Heart Association, 7272 Greenville Avenue, Dallas, TX 75231

Print ISSN: 0009-7330. Online ISSN: 1524-4571

A Novel Mouse Model of Atherosclerotic Plaque Instability for Drug Testing and Mechanistic/Therapeutic Discoveries Using Gene and MicroRNA Expression Profiling

Yung-Chih Chen, Anh Viet Bui, Jeannine Diesch, Richard Manasseh, Christian Hausding, Jennifer Rivera, Izhak Haviv, Alex Agrotis, Nay Min Htun, Jeremy Jowett, Christoph Eugen Hagemeyer, Ross D. Hannan, Alex Bobik, Karlheinz Peter

Rationale: **The high morbidity/mortality of atherosclerosis is typically precipitated by plaque rupture and consequent thrombosis. However, research on underlying mechanisms and therapeutic approaches is limited by the lack of animal models that reproduce plaque instability observed in humans.**

Objective: **Development and use of a mouse model of plaque rupture that reflects the end stage of human atherosclerosis.**

Methods and Results: **On the basis of flow measurements and computational fluid dynamics, we applied a tandem stenosis to the carotid artery of apolipoprotein E–deficient mice on high-fat diet. At 7 weeks postoperatively, we observed intraplaque hemorrhage in ≈50% of mice, as well as disruption of fibrous caps, intraluminal thrombosis, neovascularization, and further characteristics typically seen in human unstable plaques. Administration of atorvastatin was associated with plaque stabilization and downregulation of monocyte chemoattractant protein-1 and ubiquitin. Microarray profiling of mRNA and microRNA (miR) and, in particular, its combined analysis demonstrated major differences in the hierarchical clustering of genes and miRs among nonatherosclerotic arteries, stable, and unstable plaques and allows the identification of distinct genes/miRs, potentially representing novel therapeutic targets for plaque stabilization. The feasibility of the described animal model as a discovery tool was established in a pilot approach, identifying a disintegrin and metalloprotease with thrombospondin motifs 4 (ADAMTS4) and miR-322 as potential pathogenic factors of plaque instability in mice and validated in human plaques.**

Conclusions: **The newly described mouse model reflects human atherosclerotic plaque instability and represents a discovery tool toward the development and testing of therapeutic strategies aimed at preventing plaque rupture. Distinctly expressed genes and miRs can be linked to plaque instability. (*Circ Res*. 2013;113:252-265.)**

Key Words: acute myocardial infarction ■ angiogenesis ■ animal models of human disease ■ arterial thrombosis ■ atherosclerosis ■ gene expression profiling ■ inflammation ■ microRNA profiling ■ plaque rupture

Atherosclerosis, a progressive, chronic, inflammatory disease with specific, localized manifestations in the arterial wall, is a major health burden and is predicted to become the leading cause of mortality and morbidity worldwide.[1,2] Complications of atherosclerosis, such as myocardial infarction (MI), which is the largest single cause of death in developed countries, are caused by inflammation-driven rupture of atherosclerotic plaques.[3]

A major hurdle in research on mechanisms of plaque rupture is the lack of appropriate mouse models which exhibit plaque rupture and lesion characteristics of vulnerable, unstable, and thus rupture-prone plaques as found in humans.[4] Such characteristics most importantly include a thin and ruptured fibrous cap, plaque inflammation, neovascularization within the plaque (vasa vasorum), plaque hemorrhage, and intravascular (often occlusive) thrombus formation.[2,3,5–7] In addition, an animal model of plaque instability/rupture should include responsiveness to pharmacological agents known to reduce the risk of plaque rupture in humans.[8,9] Currently discussed animal models of atherosclerosis typically represent a few but not the full combination of the characteristics seen in human unstable/ruptured plaques.[10–14] An animal model of

Original received April 20, 2013; revision received May 30, 2013; accepted June 7, 2013. In May 2013, the average time from submission to first decision for all original research papers submitted to *Circulation Research* was 15 days.

From the Baker IDI Heart & Diabetes Institute, Melbourne, Australia (Y.-C.C., C.H., J.R., I.H., A.A., N.M.H., J.J., C.E.H., A.B., K.P.); Department of Medicine, Monash University, Melbourne, Australia (Y.-C.C., A.A., N.M.H., C.E.H., A.B., K.P.); Fluid Dynamics Group, CSIRO Materials Science and Engineering, Melbourne, Australia (A.V.B., R.M.); and Growth Regulation Laboratory, Peter MacCallum Cancer Centre, Melbourne, Australia (J.D., R.D.H.).

In memory of Dr Jowett.

The online-only Data Supplement is available with this article at http://circres.ahajournals.org/lookup/suppl/doi:10.1161/CIRCRESAHA.113.301562/-/DC1.

Correspondence to Karlheinz Peter, MD, PhD, Atherothrombosis and Vascular Biology, Baker IDI Heart and Diabetes Institute, PO Box 6492, St Kilda Rd Central, Melbourne, Victoria 8008, Australia. E-mail karlheinz.peter@bakeridi.edu.au

Nonstandard Abbreviations and Acronyms

ApoE$^{-/-}$	apolipoprotein E–deficient
CFD	computational fluid dynamics
HFD	high-fat diet
IH	intraplaque hemorrhage
MI	myocardial infarction
miR	microRNA
MMP	matrix metalloproteinase
TS	tandem stenosis

plaque rupture that is more representative of human plaque pathology would enable long-awaited further progress in the understanding of plaque rupture and the development of imaging tools to detect vulnerable, rupture-prone atherosclerotic plaques.[15]

It is well known that atherosclerotic plaques in humans preferentially occur at vessel bifurcations, where shear stress is low in magnitude and varies significantly over a small distance.[16] Similar predilections for atherosclerosis toward low shear stress areas have been seen in apolipoprotein E–deficient (ApoE$^{-/-}$) mice on high-fat diet (HFD).[17] Mechanistic investigations on atherosclerotic plaque development indicate that low shear stress increases the accumulation of macrophages and other inflammatory cells, stimulates overexpression of adhesion molecules and proteases, reduces stabilizing collagen fibers, increases necrotic core volume, causes thinning of fibrous caps, reduces endothelial cell coverage, and worsens lipid accumulation.[18] However, low shear stress alone does not seem to be sufficient to induce plaque rupture.[19] Tensile stress, which indeed is higher by several magnitudes than wall shear stress, seems to be an important determinant responsible for causing a vulnerable atherosclerotic plaque to rupture.[19] There is a high prevalence of plaque rupture in the proximal coronary arteries, where the tensile stress is higher compared with the periphery of the coronary artery system.[3] On the basis of these observations, we used computational fluid dynamics (CFD) to develop an animal model of plaque rupture, which combines low wall shear stress and high tensile stress. We used surgery to introduce a tandem stenosis (TS) in the carotid artery of ApoE$^{-/-}$ mice fed a HFD. Using histology, expression profiling, hierarchical clustering, and quantitative polymerase chain reaction (PCR), as well as pharmacological intervention, we provide evidence that atherosclerotic plaques in this new mouse model resemble human vulnerable plaques. In addition, we present evidence that this mouse model can be used to define and discover novel pathophysiological mechanisms relevant to atherosclerotic plaque rupture in humans.

Methods

A detailed description of methods and materials is provided in the Online Data Supplement.

TS Surgery

At 12 weeks of age, 6 weeks after commencement of HFD, ApoE$^{-/-}$ mice (C57BL/6J background) were anaesthetized by ketamine (100 mg/kg) and xylazine (10 mg/kg) mixture through intraperitoneal injection. An incision was made in the neck and the right common carotid artery was dissected from circumferential connective tissues. A TS with 150 μm (or 450 μm) outer diameters was introduced with the distal point 1 mm from the carotid artery bifurcation and the proximal point 3 mm from the distal stenosis. The stenosis diameter was obtained by placing a 6-0 blue braided polyester fiber suture around the carotid artery together with a 150- or 450-μm needle that was tied to it and later removed. Animals were euthanized at 2, 4, 7, and 11 weeks after surgery.

Statistical Analysis

Quantitative results are expressed as mean±SEM. Comparisons of parameters among 2 groups were made by the unpaired Student *t* test or Mann–Whitney test. Comparisons of parameters among 4 or 5 groups were made by 1-way ANOVA followed by post hoc analysis using the Newman–Keuls test. Data presented in the Table were evaluated using the Fisher exact test. A P value of <0.05 was considered to be statistically significant.

Results

CFD Predicts Low Shear and High Tensile Stress in a Carotid Artery TS Model

As a first step to developing an animal model of atherosclerosis that results in plaque rupture, we used CFD to predict a carotid stenosis that would generate both low shear and high tensile stress.[20] We simulated pulsatile rather than nonpulsatile, steady blood flow as conventionally done. In CFD modeling the left carotid artery, which is typically plaque free because of high and laminar flow, was used as a control (Figure 1G). A model using TS with an outer diameter of 150 μm provided the appropriate wall shear stress during both diastole (Figure 1A) and systole (Figure 1C). In comparison, a single stenosis of the same outer diameter (Figure 1B and 1D) exhibited a higher flow rate and higher wall shear stress. Our CFD calculations indicated a reduction in shear stress of ≈27% in the single stenosis model, compared with 74% in the TS model, consistent with reductions in flow in the carotid arteries of mice measured in vivo using an ultrasound Doppler probe (Figure 1F). Ultrasound flow measurements revealed a 65±4% flow reduction induced by the TS model, compared with a 26±3.3%

Table. Plaque Characteristics in Vessel Segment I

	150 μm TS (n=75)	450 μm TS (n=14)	Sham TS (n=16)	150 μm TS+Atorvastatin 10 mg/kg (n=8)	150 μm SS (n=21)
Plaque development	100% (75/75)	14% (2/14)*	0% (0/16)*	100% (8/8)	100% (21/21)
Intraplaque hemorrhage	50.6% (38/75)	0% (0/14)*	0% (0/16)*	12.5% (1/8)*	14.2% (3/21)*
Disruption of cap	32% (24/75)	0% (0/14)	0% (0/16)	12.5% (1/8)	0% (0/21)

TS indicates tandem stenosis; and SS, single stenosis.

*$P<0.05$ compare with 150 μm TS.

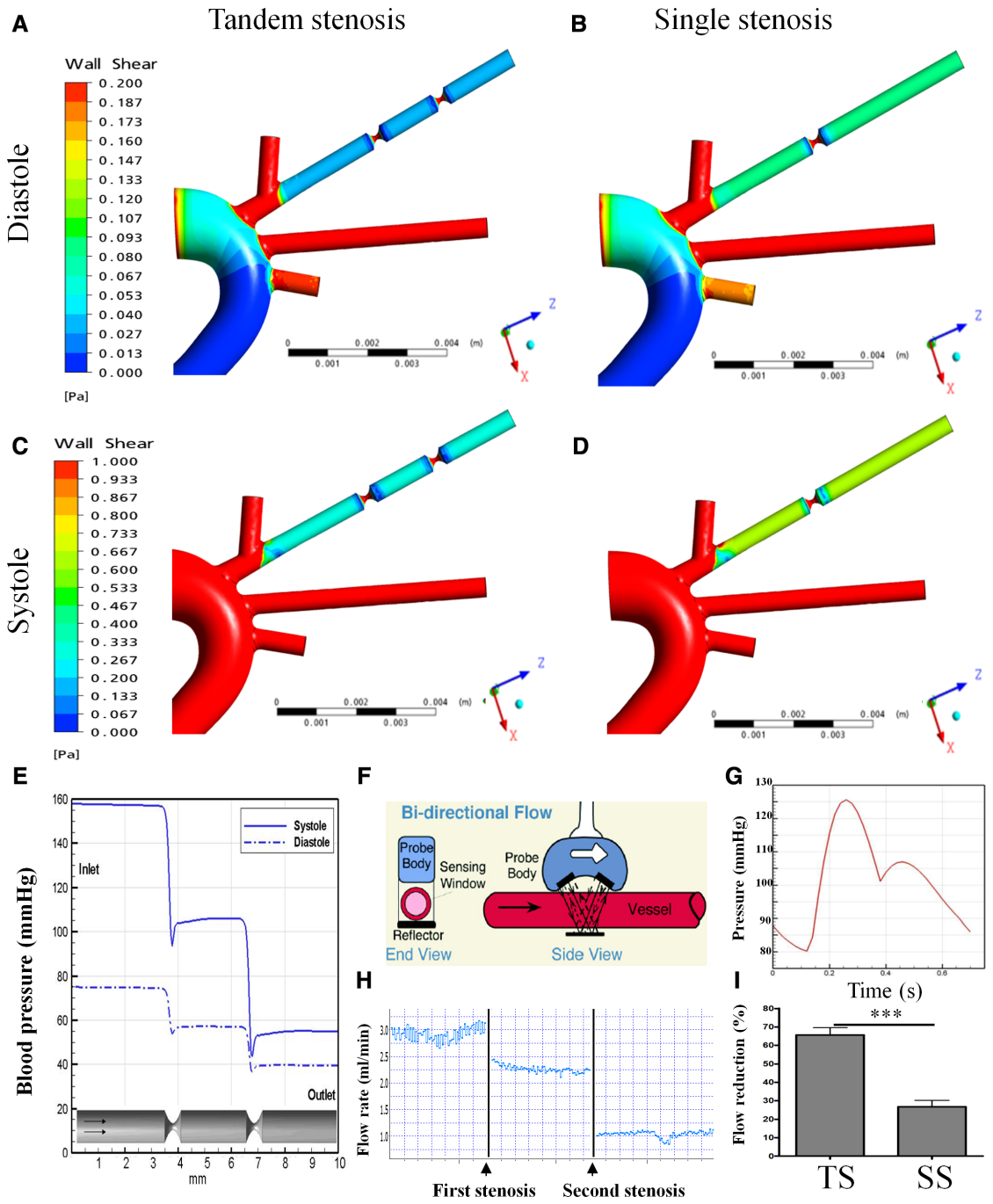

Figure 1. Computational fluid dynamics (CFD) predicts low shear and high tensile stress in a carotid artery tandem stenosis (TS) mouse model. A, During diastole, CFD demonstrates a significant reduction of wall shear stress in the TS compared with the (**B**) single stenosis (SS) model. **C** and **D**, Similar results were found during systole. **E**, The blood pressures in the TS model demonstrate that the vessel segment upstream of the proximal stenosis endures the highest tensile stress, whereas the TS model results in an overall strong reduction of flow rate and thus low wall shear stress. **F**, In vivo ultrasonic flow measurements quantifying the low flow rate in the TS model. A nano-Doppler flow probe was positioned over the artery and the carotid blood flow was measured by a flowmeter. **G**, The CFD pressure profile of pulsatile flow against time in the nonstenosed carotid artery. **H**, Blood flow rate was measured continuously during the introduction of stenoses. **I**, The percentage of reduction in flow as the change from baseline of the nonstenotic blood flow in the single and TS model (mean±SEM; n=20). Each unit represents 1 minute. Data were analyzed by a Mann–Whitney test (***P<0.001).

reduction induced by single stenosis (Figure 1I). A typical flow drop generated by the TS is shown in Figure 1H. A control group of nonconstrictive TS (450 μm outer diameter) was also examined. Flow measurements indicated no change of blood flow (data not shown). Tensile stress in the TS model was highest upstream of the proximal stenosis (Figure 1E).

Mouse TS Model Exhibits Unstable (Segments I and II) and Stable (Segments III and V) Atherosclerotic Plaques, As Well As Nonatherosclerotic Segments (Segment IV)

We next examined whether TS in the right carotid artery of ApoE$^{-/-}$ mice results in unstable atherosclerotic plaques.

After HFD of 6 weeks, TS was surgically introduced on the right carotid artery of 12-week-old ApoE$^{-/-}$ mice. Animals were euthanized after a further 7 weeks. To determine how the TS affects development of atherosclerotic lesions, the arterial system in the vicinity of the TS was divided into 5 segments and assessed histologically (Figure 2A); vessel segment I typically displayed the characteristics of atherosclerotic plaque instability/rupture, typified by disruption of fibrous caps, intraplaque hemorrhage (IH), and intraluminal thrombosis (Figure 2B). Segment I also demonstrated thin caps in the shoulder region (thin cap fibroatheroma) with large necrotic cores (Figure 2C). A representative image of the gross anatomy of the TS model indicates the atherosclerotic plaque hemorrhage in segment I (Figure 2D). Vessel segment II exhibited a yellow plaque phenotype containing intact fibrous cap with highly cellular plaques and extensive outward remodeling (Figure 2E). Vessel segment III displayed a stable atherosclerotic plaque phenotype containing intact and highly cellular fibrous caps and small cholesterol crystals (Figure 2F). Vessel segment IV was plaque free and thus representative of a nonatherosclerotic vessel (Figure 2G). Vessel segment V, which is composed of the whole aortic arch including the proximal areas of the A. brachiocephalica, A. carotis, and A. subclavia, contained stable atherosclerotic plaques characterized by thick fibrous caps with numerous smooth muscle cells, but no luminal thrombi (Figure 2H).

Unstable Plaques in the TS Mouse Atherosclerosis Model Are Associated With Intraplaque Hemorrhage (IH), Large Necrotic Cores, Rupture of Fibrous Caps, and Luminal Thrombosis

As atherosclerotic lesions in segment I of the TS model exhibited features of plaque instability, we characterized plaque progression in this segment at 2, 4, 7, and 11 weeks. Two weeks after TS surgery, segment I contained intact, stable atherosclerotic plaques that were strongly positive for CD68^{+} macrophages and for vascular cell adhesion molecule-1 expression (Online Figure I). At 4 weeks, cellular and thick fibrous caps covered most of the lesion, which contained large necrotic cores with cholesterol clefts (Figure 3A). At the shoulder region, the cap was less cellular, suggesting susceptibility to plaque rupture (Figure 3A). At 7 weeks, evidence of ruptured fibrous caps, IH, and luminal thrombi was found (Figures 2B and 3B). As these lesions progressed, there was evidence of further thinning and disruption of fibrous caps, as well as IH in the necrotic core at 11 weeks (Figure 3C; Online Figure II).

Luminal thrombosis is an important characteristic of human plaque rupture, which is absent in other mouse models.[21,22] To confirm intraluminal thrombosis, we stained for the 2 major components of clots, platelets (CD41), and fibrin. At 7 weeks, positive CD41 (Figure 3D) and fibrin (Figure 3E) staining were present within intraluminal thrombi in segment I. The fibrillar structure of fibrin can be seen at higher magnification (Figure 3F).

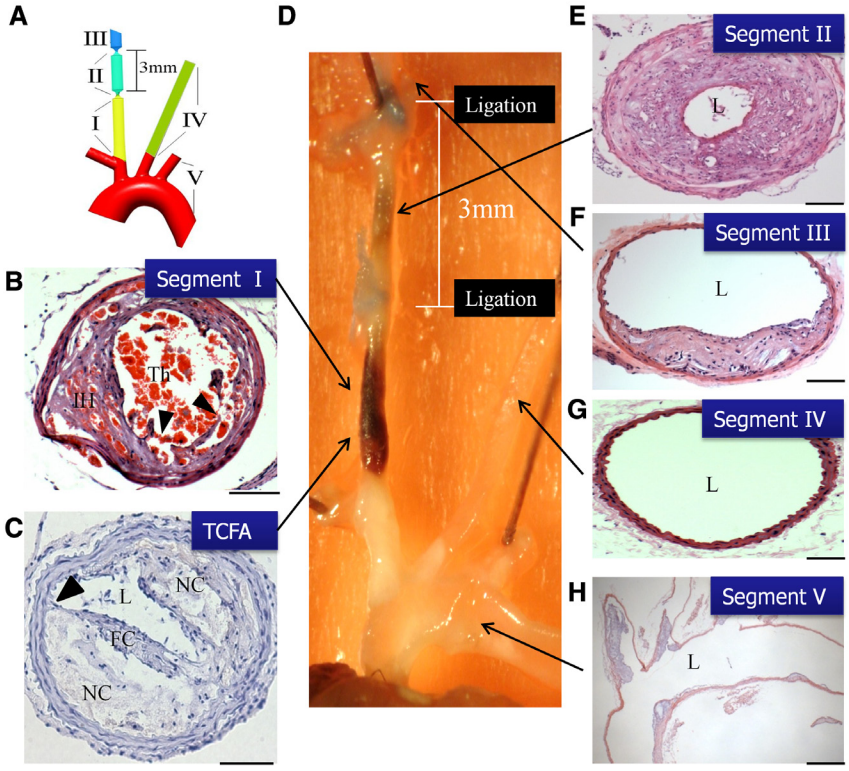

Figure 2. Cross-section of different vessel segments representing healthy, nonatherosclerotic areas and areas of stable and unstable atherosclerosis. **A**, Schematic drawing of the different vessel segments investigated in the described tandem stenosis (TS) model. **B**, Vessel segment I represents unstable/rupture-prone atherosclerotic plaques characterized by disruption of fibrous caps and luminal thrombosis. **C**, Representative thin cap fibroatheroma (TCFA) prone to rupture as typically seen in vessel segment I. **D**, Representative gross anatomy after 7 weeks after TS surgery at the depicted vessel segments. The ligation suture is blue. **E**, Vessel segment II often contains intact thin fibrous caps with highly cellular content. **F**, Vessel segment III exhibits a stable atherosclerotic phenotype containing thick fibrous caps and small necrotic cores. **G**, Vessel segment IV represents plaque-free healthy vasculature. **H**, Vessel segment V contains the aortic arch and adjacent vessel segments. The plaque phenotype shows a stable atherosclerotic plaque characterized by thick caps, which consist of fibrous tissue and smooth muscle cells. Luminal thrombi were not found in this segment. Bars indicate 100 μm in **B**, **C**, and **E**–**G**, and 1000 μm in **H**. All histological pictures depict hematoxylin and eosin staining, except **C** which depicts hematoxylin staining. FC indicates fibrous cap; IH, intraplaque hemorrhage; L, lumen; NC, necrotic core; and Th, thrombus.

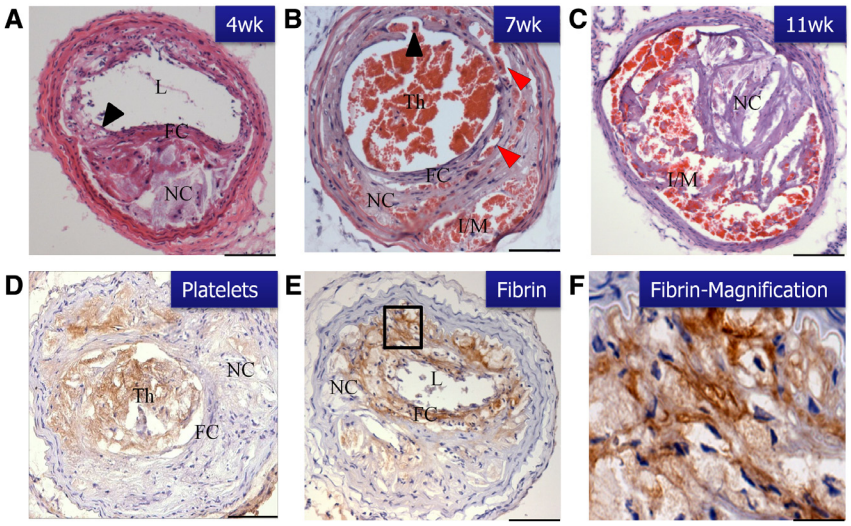

Figure 3. Typical features of plaque instability in segment I of the tandem stenosis (TS) mouse model, including luminal thrombosis, disruption of fibrous caps, fibrin deposition, intraplaque hemorrhage, and necrotic cores. A, A cross-section at 4 weeks after TS surgery, demonstrating a fibrous cap covering a large necrotic core. Arrow points to a largely acellular region in the fibrous cap susceptible to rupture. **B**, Lesion at 7 weeks after TS surgery demonstrating rupture of the fibrous cap, accompanied by occlusive luminal thrombosis (black arrow indicates the rupture site), intraplaque hemorrhage (red arrows), together with intima-media dissection. **C**, Lesion progression with lumen narrowing and blood intrusion into the necrotic core at 11 weeks after TS surgery (intimal media dissection). **D**, Luminal anti-CD41 and (**E**) anti-fibrin staining depict the presence of thrombus in the vessel lumen after plaque rupture. **F**, High power view of fibrin staining reveals its fibrillar structure. Bars indicate 100 μm in **A**–**E**; 10 μm in **F**. **A**–**C**, Stained with hematoxylin and eosin. FC indicates fibrous cap; I/M, intimal media dissection; L, lumen; NC, necrotic core; and Th, thrombus.

As IH is a characteristic feature of human plaque rupture, we examined the frequency of IH in lesions at 7 weeks after TS. IH occurred in 50.6% of TS mice (Table) and was macroscopically visible in segment I (Online Figure III). Importantly, in control mice where a single stenosis (outer diameter, 150 μm) was introduced, a much lower frequency (14.2%) of IH was observed (Table). With the outer diameter of the vessel remaining at 450 μm, none of the mice exhibited IH, indicating that the suture itself does not induce IH. IH cannot be seen in the sham-operated mice, indicating the surgical procedure does not induce IH on its own (Online Figure IV). Among the 75 animals, 24 animals were found with a clearly visible disruption of the cap (Table). In addition, platelet (CD41) and fibrin staining within the atherosclerotic plaque could only be detected in unstable atherosclerotic plaques in segment I, but not in other segments, with an average of 8.5% fibrin-positive staining of the total plaque area (n=6).

Total ligation of the right carotid artery has previously been proposed as a model of unstable atherosclerosis.[23] To allow a direct comparison to the TS model, we induced a total ligation of the right carotid artery and examined atherosclerotic plaques at 7 weeks. Low levels of lipid content and low abundance of $CD68^+$ macrophages were observed in the ligated carotid artery. Moreover, plaques displayed strong collagen staining (Trichrome) and extensive neointimal hyperplasia (Online Figure V). In contrast to our TS model, total ligation did not induce the development of necrotic cores or formation of fibrous caps.

Identification of Neo Vasa Vasorum and Intraplaque Microvessel

The neo vasa vasorum in adventitial tissue of vulnerable, unstable human atherosclerotic plaques contribute to the development of complex lesions by acting as a conduit for inflammatory cells and have also been associated with IH.[24] Consequently, we examined whether vasa vasorum can be detected within vulnerable plaques in our mouse model. Vasa vasorum were readily apparent in segment I, even macroscopically (Online Figure VIA). Expression of the endothelial cell marker CD31 confirmed the presence of neo vasa vasorum within the tunica adventitia of atherosclerotic lesions (Online Figure VIB). Atherosclerotic lesions were also highly vascularized in the region adjacent to the tunica media (Online Figure VIC). These intraplaque microvessels consist of a single layer of endothelial cells (Online Figure VID) and were often adjacent to positive iron staining, reflecting old hemorrhage remnants (Online Figure VIE).[25] The average vessel density is 3 neovessels per 100 000 μm^2 total plaque area in segment I at the 7-week time point (n=10 sections from each mouse, 10 mice were used and quantified). Importantly, intraplaque neovessels could not be found in segments II to V. Thus, our unique TS animal model presents neo vessel formation in both the tunica adventitia and within the atherosclerotic plaques, which strongly reflects characteristics observed in human unstable plaques.

Pathological Description of Vessel Segments I, II, III, and V of the TS Model

To understand the pathology of the TS model further, we analyzed plaque composition in the 5 segments at 7 weeks after TS surgery. Segment I (unstable) contained ≈80% less intimal collagen compared with segments III (stable) and V (stable; Figure 4A; Online Figure VIIA). Segment I also showed increased intimal CD31 expression compared with segments III and V, indicating intraplaque microvessel formation (Figure 4B; Online Figure VIIB). Vessel segment I comprised 50% more lipid compared with segment II ($P<0.01$) and 60% more lipid compared with segment III ($P<0.001$), whereas there was no difference in lipid content between segments I and V

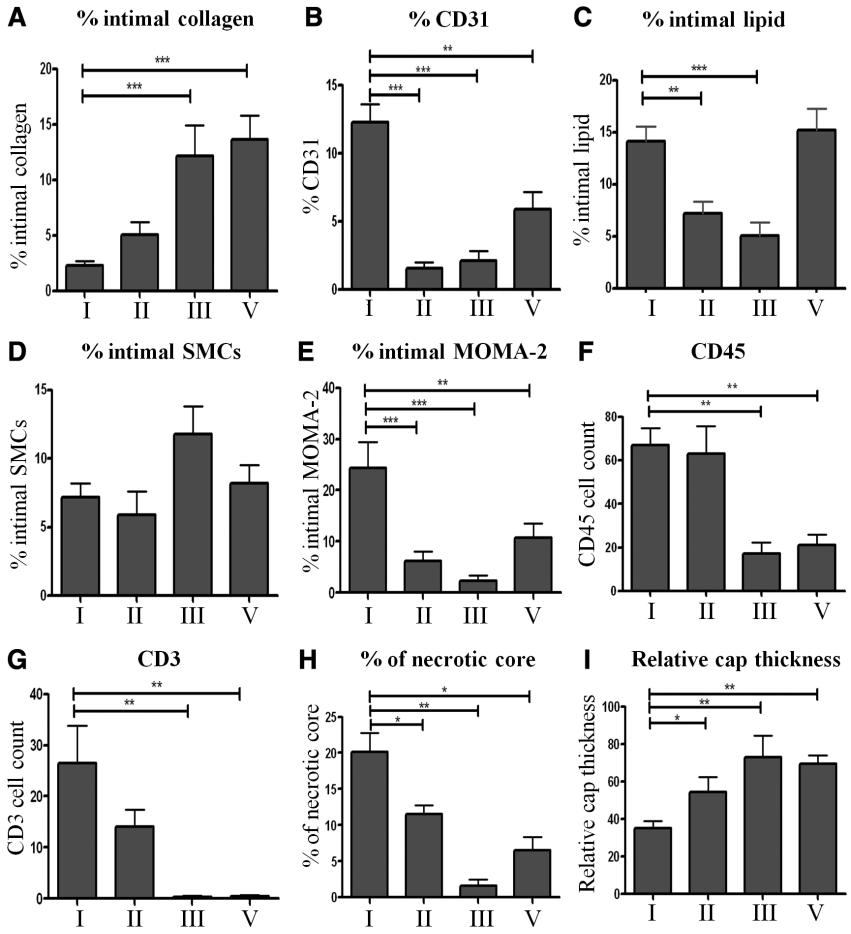

Figure 4. Pathological description of the tandem stenosis (TS) model 7 weeks after surgery. Morphometric and immunohistological analysis of collagen, CD31, lipid, smooth muscle cells (SMCs), MOMA-2, CD45, CD3, necrotic core, and relative cap thickness. **A**, The rupture-prone segment I has significantly less intimal collagen compared with the areas of stable atherosclerotic plaques (segments III and V). **B**, Segment I is highly vascularized compared with segments II, III, and V, as reflected by CD31 staining. **C**, The percentage of intimal lipid staining in segment I is significantly higher compared with segments II and III, but not to segment V. **D**, No significant difference in SMC content between the different vessel areas. **E**, Segment I contains more inflammatory macrophages as compared with segments II, III, and V, as determined by MOMA-2 staining. Segment I also contains significantly higher CD45 (**F**) and CD3 positive cells (**G**). Segment I contains the largest necrotic cores (defined by acellular area and cholesterol crystal area divided by neointimal area) compared with other fragments (**H**). Segment I exhibits the thinnest and smallest caps (as defined by relative cap thickness via the ratio of the cap thickness at the shoulder and midplaque region divided by maximal intimal cross-sectional thickness (**I**). n=12 for each group (*P<0.05; **P<0.01; and ***P<0.001).

(Figure 4C; Online Figure VIIC). Furthermore, monocyte and macrophage marker positive cells were significantly higher in segment I compared with segments II (74%), III (90%), and V (55%; Figure 4E; Online Figure VIIE). Interestingly, the number of $CD45^+$ and $CD3^+$ positive cells, representing all leukocytes and T cells, respectively, was significantly higher in segment I compared with segments III and V (Figure 4F and 4G). There was no difference in intimal smooth muscle cells, between the 5 vessel segments (Figure 4D; Online Figure VIID). Immunostaining with an IgG isotype control confirmed the specificity of the antibodies used (Online Figure VIIE, inset). Finally, unstable plaques in segment I exhibited thin cap fibroatheroma and a larger necrotic core (42%, 90%, and 65% increased necrotic core compared with segments II, III, and V, respectively; Figure 4H) and a relatively thin fibrous cap (35%, 52%, and 49% decrease in cap thickness compared with segments II, III, and V, respectively; Figure 4I). These data suggest that segment I represents an unstable atherosclerotic plaque reflecting the pathology of vulnerable plaques in humans.

Treatment With Atorvastatin Reduces the Incidence of IH

In humans, statin therapy has been shown to reduce the incidence of IH.[26] Hence, to investigate whether the unstable plaques in our TS mouse model also respond to pharmacological intervention, we evaluated the effects of statin therapy (atorvastatin 10 mg/kg per day for 7 weeks)[27] on IH induced by TS. High-density lipoprotein, low-density lipoprotein, or total cholesterol levels did not change in mice treated with atorvastatin (Online Table I). However, the incidence of spontaneous IH in segment I was substantially reduced from 50.6% to 12.5% (P<0.05; Fisher exact test; Table). To visualize the extent of IH, longitudinal sectioning of the brachiocephalic artery to the common carotid artery proximal to the first suture was performed and serial images were merged for viewing across the entire arterial segment (Figure 5A). Treatment with atorvastatin preserved the vessel lumen (Figure 5B), but there was no difference in total plaque area (Figure 5C), lipid content (Figure 5D), or foam cell accumulation (data not shown). Interestingly, atorvastatin treatment did increase collagen content (Figure 5E), indicating an increase in plaque stability.

To demonstrate further that statin treatment results in plaque-stabilizing effects in our TS mouse model, we examined 2 markers with a documented role in human plaque instability, monocyte chemoattractant protein-1 (MCP-1), and ubiquitin.[28–30] MCP-1 expression was significantly reduced by atorvastatin treatment (Figure 5F–5H). Ubiquitin was strongly expressed in the plaque area of segment I of the TS model, and this expression was significantly reduced by atorvastatin (Figure 5I–5K).

Gene Expression Profiling for Characterization of the Unstable Atherosclerotic Plaque and Identification of Genes Relevant to the Pathophysiology of Plaque Instability

Having established that the TS model shares many histopathologic features of human atherosclerosis, particularly

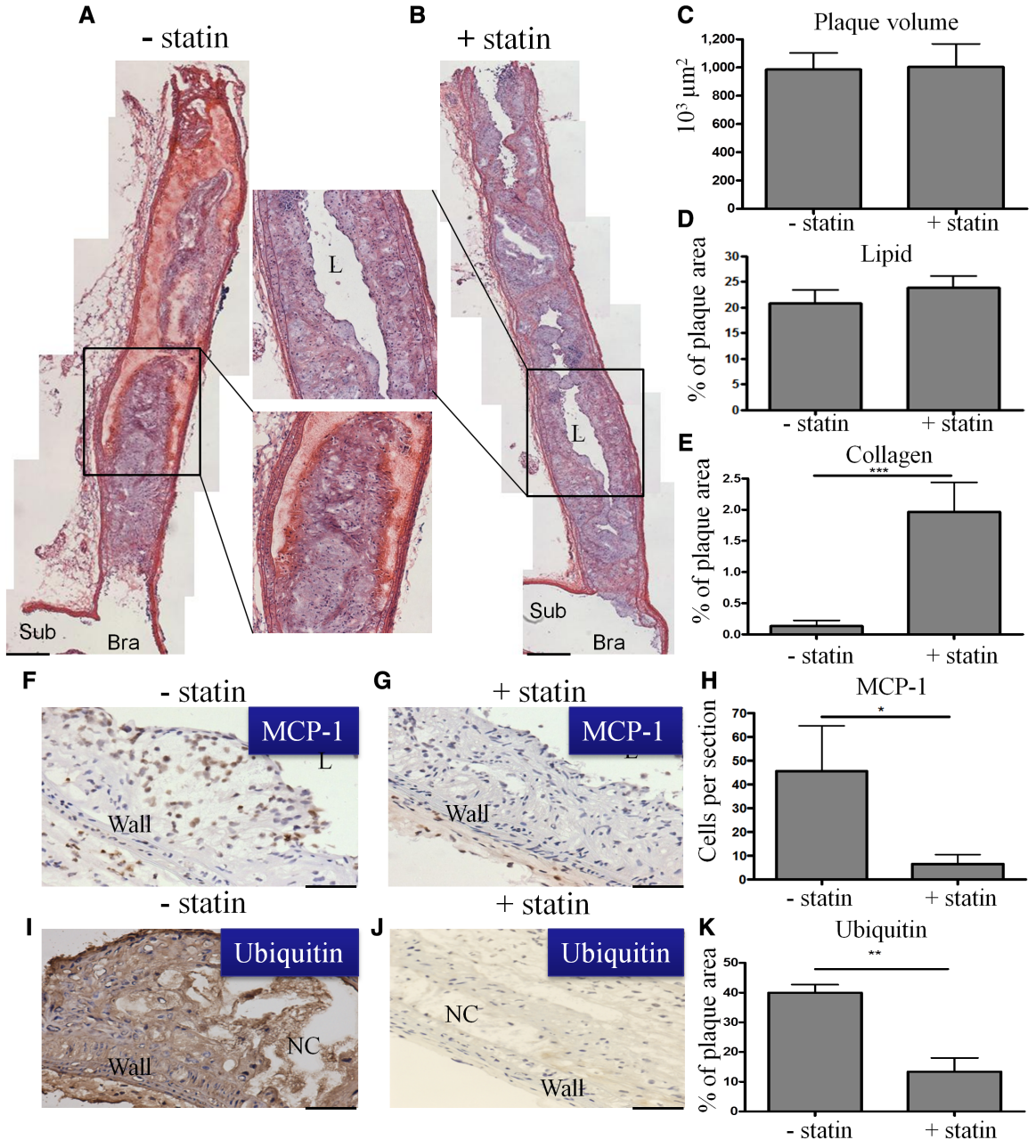

Figure 5. Atorvastatin treatment increases plaque stability and prevents intraplaque hemorrhage (IH) in the tandem stenosis (TS) mouse model at 7 weeks after surgery. Serial photos were taken and merged from the brachiocephalic artery, the right subclavian artery, and the right common carotid artery up to the proximal stenosis in the TS model. **A**, Severe IHs were typically found upstream of the proximal stenosis and were 3 to 4 mm in length. **B**, Atorvastatin-treated animals revealed significantly less IH and the vessel lumen was better preserved. **C** and **D**, Plaque size and lipid content are unchanged by atorvastatin treatment. **E**, The collagen content as assessed by picosirius red staining was substantially increased in the atorvastatin-treated vessel (n=8; $P<0.001$). **F**, The carotid artery in the TS model shows luminal narrowing and accumulation of monocyte chemoattractant protein-1 (MCP-1) positive cells adjacent to the necrotic core and fibrotic cap. **G** and **H**, The abundance of MCP-1 positive cells decreases after atorvastatin treatment (mean±SEM; n=8; $P<0.05$). **I**, Ubiquitin staining demonstrated a highly proteolytically active and inflamed plaque in the TS model. **J** and **K**, Atorvastatin treatment decreased expression of ubiquitin in the atherosclerotic plaque (mean±SEM; n=6; $P<0.01$). Bars indicate 500 µm in **A** and **B**, and 100 µm in **F**, **G**, **I**, and **J**. Bra indicates brachiocephalic artery; L, lumen; NC, necrotic core; and sub, subclavian artery.

the pathology of plaque instability, we used this model to investigate molecular characteristics associated with stable and unstable atherosclerotic plaques. We investigated gene expression in the various plaque phenotypes displayed in vessel segments I to V at 7 weeks after TS surgery. To obtain sufficient mRNA for each segment, we pooled tissue from 20 mice. As a repeat measurement, this was conducted a total of 3× (3 analyses per segment with 20 mice per analysis). Extracted RNA was processed and analyzed for gene expression using the Illumina mouse WG-6 beadchip microarray as described previously.[31] To assess the relatedness between the repeats of the same anatomic location, and thus to compare stable, unstable atherosclerotic segments and nonatherosclerotic segments with each other, we plotted

the principal component analysis of the sample profiles in an unsupervised fashion, across all genes. The principal component analysis plot clearly shows that samples pooled from identical segments were most closely related to each other, providing confidence of sample quality in each repeat (Figure 6A). Next, we performed an ANOVA, with the aim of identifying genes that were differentially expressed between stable and unstable plaques. Hierarchical clustering of genes that were differentially expressed >2-fold at $P<0.05$ significance illustrated coordinate expression patterns for each pathological sample group (Figure 6B). Several genes previously shown to be associated with plaque instability were upregulated in vessel segment I. These included MCP-1, interleukin Iβ, transforming growth factor-β, matrix metalloproteinase (MMP) 9, MMP-12, platelet-derived growth factor β, and F4/80 (Figure 6C–6I). These microarray data were confirmed by quantitative real-time PCR, demonstrating that vessel segment I had increased expression of MCP-1 (88×), interleukin Iβ (106×), transforming growth factor-β (7.8×), platelet-derived growth factor β (7.7×), MMP-9 (2.3×), MMP-12 (119×), and F4/80 (14×) when normalized to nonatherosclerotic segment IV. This demonstrates that in vessel segment I, which is prone to plaque rupture, a high degree of inflammation and protease activity is present (Figure 6C–6I, bottom).

Expression Analysis of miRs Identifies Specific Expression Profiles for Unstable Plaques (Segments I and II) and Allows the Discovery of Novel Pathophysiologically/Therapeutically Relevant miRs

MicroRNAs (miRs) are increasingly recognized as important mediators of cardiovascular pathologies.[32,33] MiR microarrays were used to demonstrate further the feasibility of our TS mouse model in discriminating between unstable and stable plaques, as well as to demonstrate the potential of the model as a discovery tool. Expression levels of miRs were determined in tissue from vessel segments I, II, IV, and V using an Illumina microarray. Hierarchical clustering of miRs that were differentially expressed >2-fold at a significance level of $P<0.05$ between any of the 4 investigated segments illustrated coordinate expression patterns, providing a strong discrimination between segments I and II compared with segments IV and V (Figure 7A). These data further support the suitability of the current mouse model to represent different plaque pathologies in different vessel segments. Notably, the miR expression profiles of segments I and II cluster close together (Figure 7A), as seen with the mRNA expression profiling (Figure 6A and 6B).

Given the strong relationship in expression profiles between segments I and II and segments IV and V, these segments were combined to represent unstable (segments I and II) or stable (segments IV and V) plaques (Online Table II). Subsequent analysis identified 30 miRs whose expression significantly differed between the 2 groups. Seven of these miRs, miR-138*, 142-3p, 298, 322, 335-3p, 450a, and 503* were chosen for validation using quantitative reverse transcriptase-PCR (Figure 7B–7H). Five of these miRs demonstrated an upregulation in segment I (unstable) when compared with segment V (stable). Among these 5 miRs, miR-322 was chosen for further exemplary analysis on the basis of its upregulation in segment I compared with segment V (Figure 7E). In addition, network analysis performed with GeneGo on predicted miR-322 target genes further supported the involvement of miR-322 in the formation of atherosclerosis, by targeting several relevant genes, such as *FGF-7*, *CX3CL1*, *FGF1*, *TNFSF13*, *APJ*, and *LAMP2* (Online Figure VIII). To confirm the relationship between miR-322 and *FGF-7*, miR-322 was transiently silenced in RAW 264.7 macrophages using anti-miR-322. This resulted in a significant increase in *FGF-7* expression (Figure 7I). In addition, the expression of anti-inflammatory cytokine *IL-10* was significantly upregulated (Figure 7J) and the expression of proinflammatory cytokine *IL-6* downregulated in response to miR-322 inhibition (Figure 7K). These data demonstrate the feasibility of the TS model as a tool for miR discovery and provide a unique and extensive list of further miRs to be studied in atherosclerosis (Online Table II).

Cross Analysis of mRNA and miR Microarray

Further analysis of the microarray expression data was performed using 2 software tools (GeneGo and Ingenuity Pathway Analysis). Segments I and II, as well as segments III, IV, and V, were grouped together to represent stable (segments III, IV, and V) or unstable plagues (segments I and II). Ingenuity Pathway Analysis clustered differentially expressed genes identified by mRNA microarrays into the main ontologies: inflammatory response, inflammatory disease, as well as cardiovascular system development and function (Online Table III). The same gene ontologies are significantly enriched when analyzing differentially expressed genes that are predicted target genes of the identified miRs (Online Table IV). A similar gene ontology profile was obtained when performing the pathway analysis using GeneGo, which demonstrated a strong overrepresentation of inflammatory response and immune response pathways in the differentially expressed genes and experimentally validated predicted miR target genes (Online Figure IXA), as well as in the differentially expressed genes, which overlap with predicted miR target genes (Online Figure IXB). Thus, microarray profiling of mRNA and miR can be used to define gene signatures that can differentiate between stable and unstable atherosclerosis in this model system. Furthermore, cross analysis of the mRNA and miR microarray data identifies gene signatures representing conserved ontologies that are associated with the atherosclerotic process, including inflammatory response and cardiovascular system and development signatures.

Overall, 243 of the predicted miR target genes overlap with differentially expressed genes identified in the mRNA microarray. Of these 243 overlapping genes, 118 show an inverse relationship with their corresponding miR. MiRs that show significant overrepresentation of their predicted, differentially expressed target genes include miR-322-5p, miR-298, miR-351, miR-138, miR-34c, or miR-503, with 47, 45, 43, 40, 34, or 23 predicted targets, respectively. These miRs are particularly attractive for further studies toward the therapeutic use of miRs in plaque stabilization.

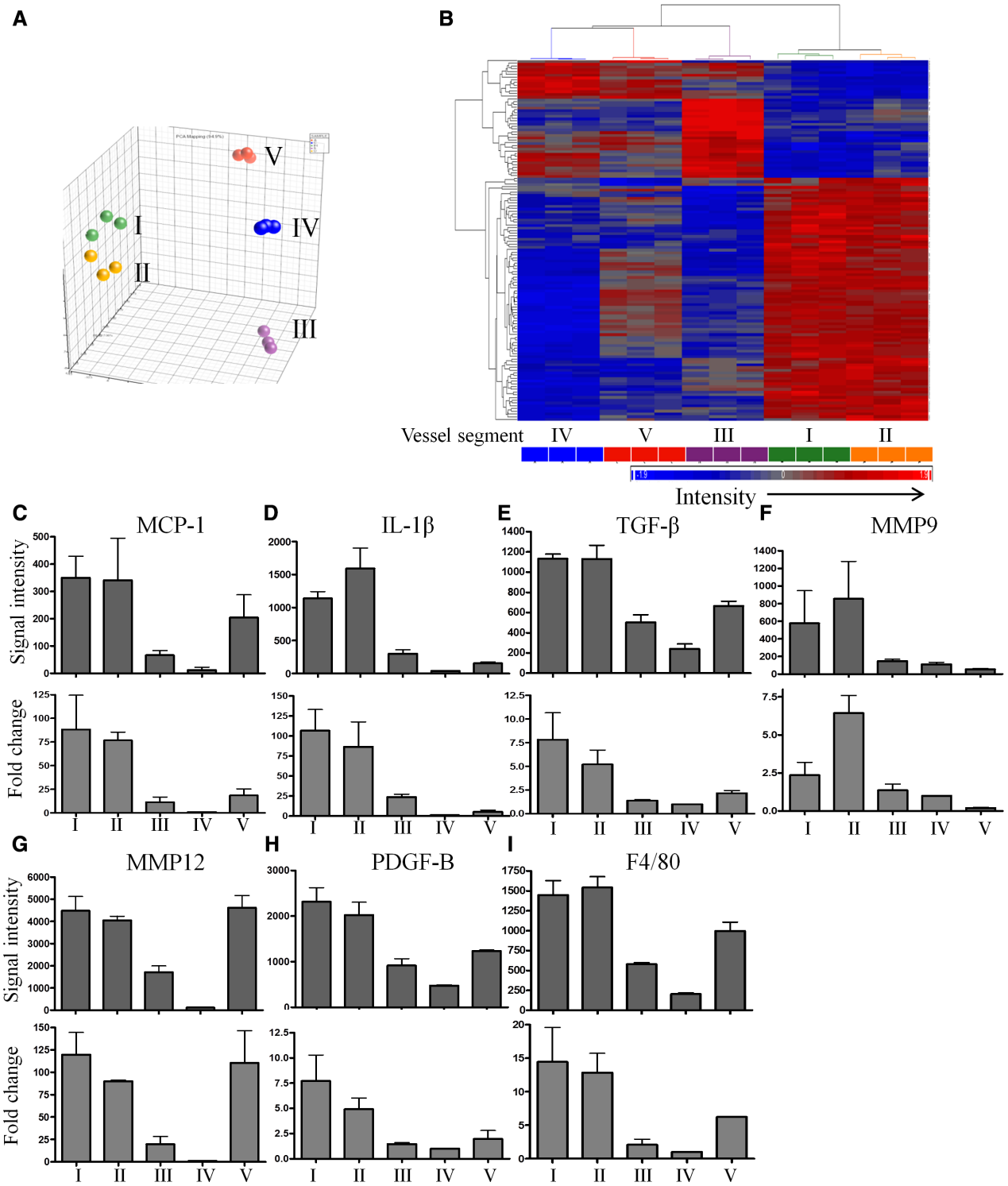

Figure 6. Microarray and quantitative reverse transcriptase polymerase chain reaction (qRT-PCR) demonstrate gene expression profiles that differentiate between unstable and stable plaques, as well as nonatherosclerotic arteries and describe the upregulation of proinflammatory and proteolytic genes. **A**, Principal component analysis demonstrates that the 3 repeats in each segment and segments I and II are closely related to each other and provide confidence of sample quality in each repeat. **B**, Analysis of the degree of coexpression of selected genes via hierarchical clustering. One hundred thirty-eight differentially expressed genes, of $P \leq 0.05$ and >2-fold change, are plotted according to their degree of respective coexpression. Columns represent vessel segments, whereas rows represent genes. Different vessel segments are listed on the bottom. Specific expression of several genes known to be proinflammatory or proteolytic and to be associated with plaque instability was also investigated in the Illumina mouse bead chip microarray. Those included are (**C**) monocyte chemoattractant protein-1 (MCP-1), (**D**) interleukin Iβ (IL Ib), (**E**) transforming growth factor-β (TGF-β), (**F**) matrix metalloproteinase (MMP) 9, (**G**) MMP 12, (**H**) platelet-derived growth factor β (PDGF-β), and (**I**) F4/80 (microarray data, **top**). For validation and exact quantification, qRT-PCR was performed and results depicted in the **bottom**. All data are normalized to 18S and expressed as fold change relative to segment IV (healthy segment). Depicted are mean±SEM.

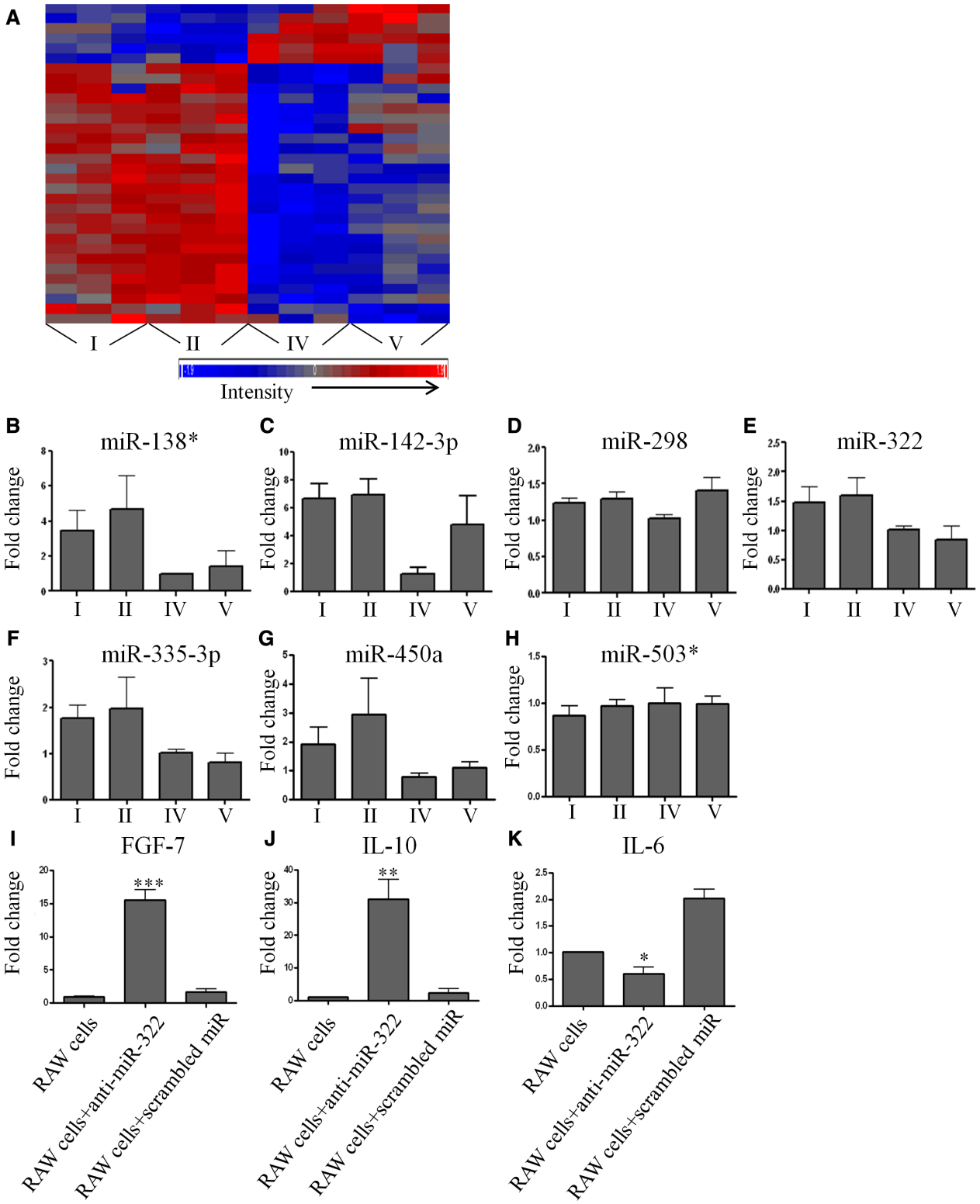

Figure 7. Microarray and quantitative reverse transcriptase polymerase chain reaction (qRT-PCR) allow identification of microRNAs (miRs), which are up- or downregulated in unstable atherosclerotic plaques and as an example points to a proinflammatory role of miR-322. A, MiR expression levels were determined in tissue from vessel segments I and II vs IV and V using the Illumina microarray beadchip. Thirty miRs differed significantly in their expression between segments IV and V and segments I and II. Heat map of these miRs, which were >2-fold differentially expressed at $P<0.05$ significance, illustrate a coordinate expression patterns for each vessel segment. MiR-138* (**B**), miR-142-3p (**C**), miR-298 (**D**), miR-322 (**E**), miR-335-3p (**F**), miR-450a (**G**), and miR-503* (**H**) were chosen for validation in qRT-PCR. MiR-322 was selected for further studies: (**I**) RAW 246.7 mouse macrophages given anti-miR-322 demonstrated the strong regulation of the expression of the target gene *FGF-7* by miR-322. **J**, Inhibition of miR-322 increases anti-inflammatory cytokine interleukin 10 (IL-10) production but inhibits (**K**) proinflammatory interleukin 6 (IL-6) cytokine generation (n=3; *$P<0.05$; **$P<0.01$; and ***$P<0.001$ compared with RAW cells only as control). All data are normalized to 18S and expressed as mean±SEM.

TS Mouse Model as Discovery Tool: Identification of ADAMTS4 As a Pathogenic Factor in Mouse and Human Plaque Instability

To demonstrate further the feasibility of the TS model as a discovery tool for the identification of genes/proteins that play an important role in plaque instability, we selected 1 gene of the 28 that were upregulated by >5-fold in the Illumina microarray (Online Table V). The Illumina microarray indicated that a disintegrin and metalloprotease with thrombospondin motifs 4 (ADAMTS4) was significantly upregulated in segment I in comparison with segment V (Online Figure XA). This upregulation was confirmed by quantitative reverse transcriptase-PCR (Online Figure XB). Immunohistochemistry localized ADAMTS4 to the fibrous cap of plaques found in segment I (Online Figure XC). The expression of ADAMTS4 was lower in plaques of the aortic arch (segment V; Online Figure XD). Next, we examined human plaques collected from patients who underwent carotid endarterectomy. We found that ADAMSTS4 was also expressed in human advanced atherosclerotic plaques (Online Figure XE). Interestingly, human early fatty streak lesions show no expression of ADAMTS4 (Online Figure XF), indicating ADAMTS4 as a marker of advanced unstable plaques. These data indicate that novel mechanisms and potential therapeutic targets relevant for plaque instability in humans can be identified using our mouse TS atherosclerosis model. This encourages the use of our unique animal model as a discovery tool for research on human plaque instability. The genes identified to be upregulated in unstable plaques (Online Table V) provide a unique basis for numerous studies toward the role of these genes in the pathogenesis of plaque rupture, as well as their suitability as potential targets for plaque stabilization.

Discussion

Rupture of atherosclerotic plaques is the major cause of mortality and morbidity of atherosclerosis in humans. For a better understanding of the underlying pathophysiology of plaque rupture, particularly for the development of drugs, which can ultimately prevent MI or stroke, an animal model is highly sought-after.[4] By focusing on hemodynamic considerations, we have designed and extensively characterized a mouse model of atherosclerosis that reflects the major characteristics of human plaque instability/rupture. Specifically, the atherosclerotic plaques of this model exhibit (1) thin and disrupted fibrous caps, (2) necrotic cores, (3) accumulation of lipids, (4) accumulation of macrophages/foam cells, (5) presence of platelets and fibrin, (6) IH, which often extended into the necrotic core, (7) intravascular thrombosis, (8) neovascularization within the plaque (notably associated with IH), (9) vascular remodeling (eccentric growth of the atheroma), (10) specific expression patterns of genes relevant to inflammation and plaque instability that strongly differentiate among unstable, stable plaques, and nonatherosclerotic arteries, (11) miR expression patterns that characterize unstable atherosclerotic plaques, (12) hemodynamic characteristics that drive and localize plaque development and instability, and (13) responsiveness to statin therapy, resulting in plaque stabilization. In addition, to demonstrate that our TS mouse model reflects the characteristics of unstable/ruptured plaques in humans, we provide proof of principle that this model can be used as a discovery tool toward a better understanding of human atherosclerotic disease and its complications.

Although the need for an animal model that reflects human plaque rupture and plaque instability is widely recognized, major controversy exists as to whether published animal models adequately reflect human plaque instability.[23,34–38] Rosenfeld et al[12] highlighted that atherosclerotic lesions in brachiocephalic arteries of mice progress from fatty streaks to advanced atheromas, characterized by highly acellular plaques. However, IHs were only present in ≤0.6% of mice investigated (>120 mice). The authors further demonstrated that this type of plaque disruption did not lead to thrombosis. Rosenfeld et al,[12] therefore, concluded that this mouse model does not reflect human plaque instability. Jackson et al[8] introduced one of the best characterized animal models focusing on the arteria brachiocephalica in ApoE$^{-/-}$ mice fed with HFD. Layers of buried/disrupted fibrous caps and erythrocyte accumulation, as well as fibrin staining, were described as an indication of previous ruptures and healing processes.[8,22] The major limitations of this model are the absence of luminal thrombosis, limited plaque inflammation, absence of vasa vasora, and the mixed genetic background of the mice used (C57BL/6 and 129).[22] Cheng et al[17] reported the use of a perivascular cast device that allows modifying shear stress in the carotid artery of mice. The authors demonstrated that low shear stress causes atherosclerotic plaques to exhibit features of a vulnerable phenotype.[18] However, the cast itself may cause an artificial inflammatory reaction and pivotal features of human vulnerable plaque development, such as the disruption of fibrous caps, necrotic cores, or any luminal thrombosis, are missing. von der Thüsen et al[10] developed an interesting but elaborate model that combines the application of a perivascular silastic carotid collar placement, the intravascular injection of a recombinant adenovirus carrying a p53 transgene, and the application of a vasopressor to achieve plaque rupture in 40% of ApoE$^{-/-}$ mice. This model by combining the induction of inflammation, apoptosis, and high tensile stress has provided major pathophysiological insights, but is not suitable as a high throughput animal model.[10] Although representing important features of plaque instability, it has also been discussed as not fully representing human atherosclerosis.[39] Notably, some mouse models were developed with a focus on individual features of plaque instability. For example, Sasaki et al[23] used a total vessel ligation to induce short-term thrombosis on the basis of blood stasis to reflect luminal thrombosis as part of human plaque development.[35] Overall, the strong medical need for an animal model of plaque instability has resulted in the development of various mouse models, but none is broadly used or has been generally accepted to represent the pathology of human vulnerable atherosclerotic lesions fully.[22]

Only a few mouse models of atherosclerosis demonstrate advanced disease in the coronary arteries.[40–42] These mouse models with genetic deficiencies (scavenger receptor class B type I and low-density lipoprotein receptor double knockout mice, V-akt thymoma viral oncogene homolog 1, and apolipoprotein E double knockout mice) have attracted major interest, particularly as they are associated with MI and premature

death. As both, histological characteristics of human vulnerable plaques and advanced occlusive coronary artery disease have been seen in these mice, it remains to be determined and is of major interest whether plaque rupture or progressive vessel occlusion is the underlying mechanism for MI and death.

In addition to thrombosis, plaque hemorrhage is the most prominent driving force of instability in human atherosclerotic plaques. The accumulation of cholesterol originating from erythrocyte membranes causes enlargement of the necrotic core, stimulates macrophage infiltration, and triggers further characteristics of plaque instability.[10,17,25] The fact that plaque hemorrhage is rare or has typically not been described in animal models of atherosclerosis to date has questioned the relevance of many models for the investigation of mechanisms in human atherosclerosis. In contrast, in our TS model, the specific detection of plaque hemorrhage in the vessel segment of plaque instability and the strong reduction of its prevalence with atorvastatin treatment indicate that this mouse model reflects human plaque pathology.

Adventitial vasa vasorum exhibit a strong association with atherosclerotic plaque development. Administration of the angiogenesis inhibitor, angiostatin, suppresses lesion growth.[43] Although a relationship exists between the function of neovessels and manifestation of atherosclerosis, its nature remains unclear. In our TS model, we observed neovascularization close to the internal elastic lamina, often associated with plaque hemorrhage, and interestingly only in unstable plaques in segment I, not in other segments. This association reflects human plaque pathology and has not been described in other mouse models of atherosclerosis. Neovessels are typically formed by endothelial cells without pericyte support, which is thought to explain their leaky nature. Again the finding of neovascularization of plaques further supports the suitability of our plaque rupture model for studies of human plaque pathology.

The plaque-stabilizing effects seen with atorvastatin, in particular the significant reduction of IH further supports the unique translational validity of TS model. Atorvastatin reduced the expression of MCP-1 and ubiquitin, proteins that are highly expressed in unstable human atherosclerotic plaques.[44] Furthermore, the detected increase in collagen expression is also a hallmark of statins' stabilizing effects on human atherosclerosis.[45] Finally, the clinically documented reduction of cardiovascular events in patients on statin therapy may be well reflected in our finding of reduced incidence of IH.[46] The ability to test pharmaceutical reagents for their effects on plaque stability/rupture opens up a wide range of applications using our TS animal model and its translation to human plaque pathology.

The use of mRNA microarray technology has provided major advances and information on plaque rupture at 3 different levels. First, the significant differences of overall gene expression between the various vessel segments provide strong support that the biology of stable and unstable atherosclerotic plaques is distinct and our animal model can be used to distinguish these differences. Interestingly, hierarchical clustering showed a strong similarity between segments I and II, indicating that the main underlying pathogenic mechanisms of plaque instability, such as inflammation, are present in both segments. However, different hemodynamic conditions seem to define differences in plaque morphology as seen between segments I and II. This supports our initial hypothesis that plaque instability is determined by specific hemodynamic conditions, and it strengthens the rationale of using a TS to create a mouse model of plaque instability. Second, mRNA expression assessed using Illumina chip technology and confirmed by quantitative reverse transcriptase-PCR demonstrated a significant upregulation of genes previously associated with human plaque instability, including MCP-1, interleukin Iβ, transforming growth factor-β, platelet-derived growth factor β, MMP-9, MMP-12, and F4/80.[47] MCP-1 has been postulated to be a direct mediator of plaque instability by inducing the expression of metalloproteinases, adhesion molecules, and cytokines. Inhibition of MCP-1 has previously been shown to induce stabilization of atherosclerotic plaques and reduce hyperplasia after balloon injury in animal models.[48,49] Similar associations have been seen in humans.[28] Furthermore, MMP-9 and 12 have been directly associated with atherosclerotic plaque development, including instability in both knockout/transgenic animals and humans.[50,51] Finally, our expression profiling studies established the TS model as a unique discovery tool. We have identified a unique list of genes that promise to be relevant to plaque instability/rupture (Online Table V). This opens up the opportunity for numerous studies to investigate the role of these genes in the pathogenesis of plaque rupture and their suitability as potential therapeutic targets for plaque stabilization.

One of the findings originating from our gene expression profiling is the upregulation of ADAMTS4 in ruptured carotid atherosclerotic plaques of mice and the direct demonstration of its relevance for human carotid plaques. Interestingly, ADAMTS4 was located in the fibrous cap adjacent to the areas of plaque rupture in the mouse. ADAMTS4 is a member of the metalloproteinase family, which includes secreted proteinases that bind to and cleave extracellular matrix components. Degradation of extracellular matrix, such as versican and collagen, has received much attention in regards to promoting plaque instability.[52] ADAMTS4 cleaves versican and has been recently identified in human atherosclerotic plaques.[53] Notably, plasma ADAMTS4 has been found to be increased in patients with acute MI.[54] Further work is warranted to address the detailed role of ADAMTS4 systematically in plaque formation and stability.

Our TS model offers the unique opportunity to identify miRs involved in plaque rupture. Although the functions of these miRs are yet to be fully elucidated, previous reports demonstrated that, for example, miR-138 and miR-142 are upregulated in blood of stroke patients.[55] MiR-322 and miR-335 have been demonstrated to promote adipogenesis by inhibiting the Wnt signaling pathway in 3T3-L1 cells.[56] This pathway demonstrates a profound involvement in regulating inflammation, foam cell accumulation, pathological angiogenesis, and atherosclerosis, roles that are also consistent with our findings. In addition, miR-322 regulates several genes involved in atherosclerosis, such as *FGF-7*, *CX3CL1*, *FGF1*, *TNFSF13*, *APJ*, and *LAMP2*. A network map of these genes, as well as other experimentally validated miR-322 target genes that were differentially expressed in unstable and stable plaque as identified by mRNA microarray, is illustrated in Online Figure VIII.

The list of miRs (Online Table II) found to be upregulated in unstable plaques provides the basis for attractive future studies aiming to define the pathophysiological role of these miRs in plaque instability/rupture, and the primary target genes through which these effects are mediated. Most intriguing is the possibility to use the recently established, highly promising therapeutic approach of antagonizing miRs[33,57] toward plaque stabilization and ultimately the prevention of MI and stroke.

A combined analysis of miR and mRNA confirms the induction of different atherosclerotic phenotypes after TS surgery and identified several novel genes and miRs differentially and inversely expressed in unstable plaques, which are potentially suitable for therapeutic approaches toward plaque stabilization. In addition, pathway analysis with Ingenuity Pathway Analysis or GeneGo revealed a significant overrepresentation of differentially expressed genes or miR target genes involved in the inflammatory response and immune response, and overall showed a strong correlation between mRNA and miR datasets, indicating the validity of our data sets.

In conclusion, we developed and characterized a novel animal model of atherosclerosis that resembles atherosclerotic plaque development seen in humans. This unique animal model is a promising tool to study mechanisms of plaque instability/rupture and to identify therapeutic targets with the ultimate aim to prevent atherosclerotic plaque rupture.

Acknowledgments

In memoriam of Dr Jowett, who sadly passed away during the work on the article revision. We are grateful to Dr Peter Tipping for his gift of an anti-mouse fibrin antibody.

Sources of Funding

This research was funded by infrastructure funding from the Victorian government and a project grant from the National Health and Medical Research Council of Australia.

Disclosures

Y.-C. Chen was supported by a Faculty Postgraduate Research Scholarship, Monash University. A. Bobik is a fellow of the National Health and Medical Research Council (NHMRC) of Australia. K. Peter is a Future fellow of the Australian Research Council and an honorary fellow of the NHMRC. The other authors report no conflict.

References

1. Lloyd-Jones D, Adams R, Carnethon M, et al; American Heart Association Statistics Committee and Stroke Statistics Subcommittee. Heart disease and stroke statistics–2009 update: a report from the American Heart Association Statistics Committee and Stroke Statistics Subcommittee. *Circulation*. 2009;119:480–486.
2. Libby P, Ridker PM, Hansson GK; Leducq Transatlantic Network on Atherothrombosis. Inflammation in atherosclerosis: from pathophysiology to practice. *J Am Coll Cardiol*. 2009;54:2129–2138.
3. Cheruvu PK, Finn AV, Gardner C, Caplan J, Goldstein J, Stone GW, Virmani R, Muller JE. Frequency and distribution of thin-cap fibroatheroma and ruptured plaques in human coronary arteries: a pathologic study. *J Am Coll Cardiol*. 2007;50:940–949.
4. Finn AV, Nakano M, Narula J, Kolodgie FD, Virmani R. Concept of vulnerable/unstable plaque. *Arterioscler Thromb Vasc Biol*. 2010;30:1282–1292.
5. Hansson GK, Libby P. The immune response in atherosclerosis: a double-edged sword. *Nat Rev Immunol*. 2006;6:508–519.
6. Thim T, Hagensen MK, Bentzon JF, Falk E. From vulnerable plaque to atherothrombosis. *J Intern Med*. 2008;263:506–516.
7. Matter CM, Stuber M, Nahrendorf M. Imaging of the unstable plaque: how far have we got? *Eur Heart J*. 2009;30:2566–2574.
8. Jackson CL, Bennett MR, Biessen EA, Johnson JL, Krams R. Assessment of unstable atherosclerosis in mice. *Arterioscler Thromb Vasc Biol*. 2007;27:714–720.
9. Arca M, Gaspardone A. Atorvastatin efficacy in the primary and secondary prevention of cardiovascular events. *Drugs*. 2007;67 (Suppl 1):29–42.
10. von der Thüsen JH, van Vlijmen BJ, Hoeben RC, Kockx MM, Havekes LM, van Berkel TJ, Biessen EA. Induction of atherosclerotic plaque rupture in apolipoprotein E-/- mice after adenovirus-mediated transfer of p53. *Circulation*. 2002;105:2064–2070.
11. Ylä-Herttuala S, Bentzon JF, Daemen M, et al. Stabilisation of atherosclerotic plaques. Position paper of the European Society of Cardiology (ESC) Working Group on atherosclerosis and vascular biology. *Thromb Haemost*. 2011;106:1–19.
12. Rosenfeld ME, Averill MM, Bennett BJ, Schwartz SM. Progression and disruption of advanced atherosclerotic plaques in murine models. *Curr Drug Targets*. 2008;9:210–216.
13. Moore KJ, Tabas I. Macrophages in the pathogenesis of atherosclerosis. *Cell*. 2011;145:341–355.
14. Rosenfeld ME, Carson KG, Johnson JL, Williams H, Jackson CL, Schwartz SM. Animal models of spontaneous plaque rupture: the holy grail of experimental atherosclerosis research. *Curr Atheroscler Rep*. 2002;4:238–242.
15. Tabas I. Pulling down the plug on atherosclerosis: finding the culprit in your heart. *Nat Med*. 2011;17:791–793.
16. Caro CG. Discovery of the role of wall shear in atherosclerosis. *Arterioscler Thromb Vasc Biol*. 2009;29:158–161.
17. Cheng C, Tempel D, van Haperen R, van der Baan A, Grosveld F, Daemen MJ, Krams R, de Crom R. Atherosclerotic lesion size and vulnerability are determined by patterns of fluid shear stress. *Circulation*. 2006;113:2744–2753.
18. Chatzizisis YS, Baker AB, Sukhova GK, Koskinas KC, Papafaklis MI, Beigel R, Jonas M, Coskun AU, Stone BV, Maynard C, Shi GP, Libby P, Feldman CL, Edelman ER, Stone PH. Augmented expression and activity of extracellular matrix-degrading enzymes in regions of low endothelial shear stress colocalize with coronary atheromata with thin fibrous caps in pigs. *Circulation*. 2011;123:621–630.
19. Slager CJ, Wentzel JJ, Gijsen FJ, Thury A, van der Wal AC, Schaar JA, Serruys PW. The role of shear stress in the destabilization of vulnerable plaques and related therapeutic implications. *Nat Clin Pract Cardiovasc Med*. 2005;2:456–464.
20. Slager CJ, Wentzel JJ, Gijsen FJ, Schuurbiers JC, van der Wal AC, van der Steen AF, Serruys PW. The role of shear stress in the generation of rupture-prone vulnerable plaques. *Nat Clin Pract Cardiovasc Med*. 2005;2:401–407.
21. Arbustini E, Dal Bello B, Morbini P, Burke AP, Bocciarelli M, Specchia G, Virmani R. Plaque erosion is a major substrate for coronary thrombosis in acute myocardial infarction. *Heart*. 1999;82:269–272.
22. Schwartz SM, Galis ZS, Rosenfeld ME, Falk E. Plaque rupture in humans and mice. *Arterioscler Thromb Vasc Biol*. 2007;27:705–713.
23. Sasaki T, Kuzuya M, Nakamura K, Cheng XW, Shibata T, Sato K, Iguchi A. A simple method of plaque rupture induction in apolipoprotein E-deficient mice. *Arterioscler Thromb Vasc Biol*. 2006;26:1304–1309.
24. Giannoni MF, Vicenzini E. Focus on the "unstable" carotid plaque: detection of intraplaque angiogenesis with contrast ultrasound. Present state and future perspectives. *Curr Vasc Pharmacol*. 2009;7:180–184.
25. Michel JB, Virmani R, Arbustini E, Pasterkamp G. Intraplaque haemorrhages as the trigger of plaque vulnerability. *Eur Heart J*. 2011;32:1977–85, 1985a, 1985b, 1985c.
26. Jain MK, Ridker PM. Anti-inflammatory effects of statins: clinical evidence and basic mechanisms. *Nat Rev Drug Discov*. 2005;4:977–987.
27. Nachtigal P, Pospisilova N, Jamborova G, Pospechova K, Solichova D, Andrys C, Zdansky P, Micuda S, Semecky V. Atorvastatin has hypolipidemic and anti-inflammatory effects in apoE/LDL receptor-double-knockout mice. *Life Sci*. 2008;82:708–717.
28. Ikeda U, Matsui K, Murakami Y, Shimada K. Monocyte chemoattractant protein-1 and coronary artery disease. *Clin Cardiol*. 2002;25:143–147.
29. Herrmann J, Edwards WD, Holmes DR Jr, Shogren KL, Lerman LO, Ciechanover A, Lerman A. Increased ubiquitin immunoreactivity in unstable atherosclerotic plaques associated with acute coronary syndromes. *J Am Coll Cardiol*. 2002;40:1919–1927.
30. Versari D, Herrmann J, Gössl M, Mannheim D, Sattler K, Meyer FB, Lerman LO, Lerman A. Dysregulation of the ubiquitin-proteasome

system in human carotid atherosclerosis. *Arterioscler Thromb Vasc Biol*. 2006;26:2132–2139.
31. Matthews VB, Allen TL, Risis S, Chan MH, Henstridge DC, Watson N, Zaffino LA, Babb JR, Boon J, Meikle PJ, Jowett JB, Watt MJ, Jansson JO, Bruce CR, Febbraio MA. Interleukin-6-deficient mice develop hepatic inflammation and systemic insulin resistance. *Diabetologia*. 2010;53:2431–2441.
32. Bauersachs J, Thum T. Biogenesis and regulation of cardiovascular microRNAs. *Circ Res*. 2011;109:334–347.
33. Small EM, Olson EN. Pervasive roles of microRNAs in cardiovascular biology. *Nature*. 2011;469:336–342.
34. Johnson J, Carson K, Williams H, Karanam S, Newby A, Angelini G, George S, Jackson C. Plaque rupture after short periods of fat feeding in the apolipoprotein E-knockout mouse: model characterization and effects of pravastatin treatment. *Circulation*. 2005;111:1422–1430.
35. Ni M, Chen WQ, Zhang Y. Animal models and potential mechanisms of plaque destabilisation and disruption. *Heart*. 2009;95:1393–1398.
36. Gough PJ, Gomez IG, Wille PT, Raines EW. Macrophage expression of active MMP-9 induces acute plaque disruption in apoE-deficient mice. *J Clin Invest*. 2006;116:59–69.
37. de Nooijer R, Verkleij CJ, von der Thüsen JH, Jukema JW, van der Wall EE, van Berkel TJ, Baker AH, Biessen EA. Lesional overexpression of matrix metalloproteinase-9 promotes intraplaque hemorrhage in advanced lesions but not at earlier stages of atherogenesis. *Arterioscler Thromb Vasc Biol*. 2006;26:340–346.
38. Clarke MC, Figg N, Maguire JJ, Davenport AP, Goddard M, Littlewood TD, Bennett MR. Apoptosis of vascular smooth muscle cells induces features of plaque vulnerability in atherosclerosis. *Nat Med*. 2006;12:1075–1080.
39. Majesky MW. Mouse model for atherosclerotic plaque rupture. *Circulation*. 2002;105:2010–2011.
40. Braun A, Trigatti BL, Post MJ, Sato K, Simons M, Edelberg JM, Rosenberg RD, Schrenzel M, Krieger M. Loss of SR-BI expression leads to the early onset of occlusive atherosclerotic coronary artery disease, spontaneous myocardial infarctions, severe cardiac dysfunction, and premature death in apolipoprotein E-deficient mice. *Circ Res*. 2002;90:270–276.
41. Fernández-Hernando C, József L, Jenkins D, Di Lorenzo A, Sessa WC. Absence of Akt1 reduces vascular smooth muscle cell migration and survival and induces features of plaque vulnerability and cardiac dysfunction during atherosclerosis. *Arterioscler Thromb Vasc Biol*. 2009;29:2033–2040.
42. Fernández-Hernando C, Ackah E, Yu J, Suárez Y, Murata T, Iwakiri Y, Prendergast J, Miao RQ, Birnbaum MJ, Sessa WC. Loss of Akt1 leads to severe atherosclerosis and occlusive coronary artery disease. *Cell Metab*. 2007;6:446–457.
43. Moulton KS, Vakili K, Zurakowski D, Soliman M, Butterfield C, Sylvin E, Lo KM, Gillies S, Javaherian K, Folkman J. Inhibition of plaque neovascularization reduces macrophage accumulation and progression of advanced atherosclerosis. *Proc Natl Acad Sci U S A*. 2003;100:4736–4741.
44. Herrmann J, Soares SM, Lerman LO, Lerman A. Potential role of the ubiquitin-proteasome system in atherosclerosis: aspects of a protein quality disease. *J Am Coll Cardiol*. 2008;51:2003–2010.
45. Rosenson RS. Pluripotential mechanisms of cardioprotection with HMG-CoA reductase inhibitor therapy. *Am J Cardiovasc Drugs*. 2001;1:411–420.
46. Schoenhagen P, Tuzcu EM, Apperson-Hansen C, Wang C, Wolski K, Lin S, Sipahi I, Nicholls SJ, Magyar WA, Loyd A, Churchill T, Crowe T, Nissen SE. Determinants of arterial wall remodeling during lipid-lowering therapy: serial intravascular ultrasound observations from the Reversal of Atherosclerosis with Aggressive Lipid Lowering Therapy (REVERSAL) trial. *Circulation*. 2006;113:2826–2834.
47. Koenig W, Khuseyinova N. Biomarkers of atherosclerotic plaque instability and rupture. *Arterioscler Thromb Vasc Biol*. 2007;27:15–26.
48. Inoue S, Egashira K, Ni W, Kitamoto S, Usui M, Otani K, Ishibashi M, Hiasa K, Nishida K, Takeshita A. Anti-monocyte chemoattractant protein-1 gene therapy limits progression and destabilization of established atherosclerosis in apolipoprotein E-knockout mice. *Circulation*. 2002;106:2700–2706.
49. Kitamoto S, Egashira K. Gene therapy targeting monocyte chemoattractant protein-1 for vascular disease. *J Atheroscler Thromb*. 2002;9:261–265.
50. Galis ZS, Sukhova GK, Lark MW, Libby P. Increased expression of matrix metalloproteinases and matrix degrading activity in vulnerable regions of human atherosclerotic plaques. *J Clin Invest*. 1994;94:2493–2503.
51. Ye S. Influence of matrix metalloproteinase genotype on cardiovascular disease susceptibility and outcome. *Cardiovasc Res*. 2006;69:636–645.
52. Galis ZS, Khatri JJ. Matrix metalloproteinases in vascular remodeling and atherogenesis: the good, the bad, and the ugly. *Circ Res*. 2002;90:251–262.
53. Wågsäter D, Björk H, Zhu C, Björkegren J, Valen G, Hamsten A, Eriksson P. ADAMTS-4 and -8 are inflammatory regulated enzymes expressed in macrophage-rich areas of human atherosclerotic plaques. *Atherosclerosis*. 2008;196:514–522.
54. Zha Y, Chen Y, Xu F, Li T, Zhao C, Cui L. ADAMTS4 level in patients with stable coronary artery disease and acute coronary syndromes. *Biomed Pharmacother*. 2010;64:160–164.
55. Tan KS, Armugam A, Sepramaniam S, Lim KY, Setyowati KD, Wang CW, Jeyaseelan K. Expression profile of MicroRNAs in young stroke patients. *PLoS One*. 2009;4:e7689.
56. Qin L, Chen Y, Niu Y, Chen W, Wang Q, Xiao S, Li A, Xie Y, Li J, Zhao X, He Z, Mo D. A deep investigation into the adipogenesis mechanism: profile of microRNAs regulating adipogenesis by modulating the canonical Wnt/beta-catenin signaling pathway. *BMC Genomics*. 2010;11:320.
57. van Rooij E, Olson EN. MicroRNA therapeutics for cardiovascular disease: opportunities and obstacles. *Nat Rev Drug Discov*. 2012;11:860–872.

Novelty and Significance

What Is Known?

- Rupture of unstable atherosclerotic plaques, which can result in acute myocardial infarction or stroke, is a leading cause of mortality and morbidity.
- Low wall shear stress and high tensile stress are major determinants of the formation of unstable, rupture-prone plaques.
- Research on mechanisms and therapeutic strategies is hampered by lack of an animal model that adequately reflects human plaque instability.

What New Information Does This Article Contribute?

- Surgically applied tandem stenosis of the carotid artery of apolipoprotein E–deficient mice creates a combination of low shear stress and high tensile stress, leading to unstable, vulnerable atherosclerotic plaque development, including plaque rupture, which closely resembles human plaque instability.
- The tandem stenosis model represents a unique discovery platform for identification of clinically relevant pathogenic factors, including microRNAs, and for the development and testing of potential therapeutics that can prevent plaque instability/rupture.

Although the major complication of atherosclerosis is plaque rupture, there is no animal model that fully reflects final stages of human plaque instability and rupture. On the basis of computational fluid dynamics, we used a surgically applied tandem stenosis to create a low shear/high tensile stress–defined vessel segment in the carotid artery of apolipoprotein E–deficient mice. This facilitates the formation of unstable plaques with characteristics that reflect human plaque pathology, including plaque rupture. Profiling of unstable plaques from this model led to the identification of several pathways, genes and microRNAs potentially involved in human plaque instability. Furthermore, as demonstrated with atorvastatin, the novel model could also be used for drug testing. This mouse model of plaque instability/rupture represents a unique discovery tool that allows for identification of pathogenic factors and development and testing of drugs, ultimately facilitating the development of new strategies for the treatment of plaque instability and prevention of plaque rupture.

Supplemental Material

Online Material and Methods

Numerical simulation of computational fluid dynamic (CFD)

The computational domain comprising the aortic arch and the artery with artificially created stenoses was constructed based on physiological and medical imaging data using the ANSYS Design Modeler 11. The computational grid consisted of approximately 150,000 tetrahedral/hexagonal elements grid refinement near the wall. The fluid medium was assumed to be Newtonian and have a constant density and viscosity equal to 1060 kg/m^3 and 0.0036 Pa·s, respectively. The blood flow was considered as three dimensional and pulsatile with the flow inlet boundary conditions simulated as mouse cardiac output. To obtain the flow velocity and pressure distributions in this model, the flow (Navier-Stokes) equations were solved with use of the finite-element commercial CFD software ANSYS CFX 11.

Mice

Male ApoE-deficient ($ApoE^{-/-}$) mice on a C57BL/6J background were obtained from the Animal Resource Centre in Western Australia. The $ApoE^{-/-}$ mice were backcrossed to C57BL/6J for at least 10x. In total, 250 $ApoE^{-/-}$ mice were used in this study and allocated into each group e.g. 150µm TS, 450µm TS, sham TS, 150µm TS plus atorvastatin, 150µm SS). Mice at 6 weeks of age were assigned randomly to one of these groups. Mice then fed a HFD containing 22% fat and 0.15% cholesterol (SF00-219, Specialty Feeds, Western Australia) for 6 weeks before TS surgery. At 12 weeks of age, TS were introduced into the mice. For the atorvastatin group, 8 mice were given Lipitor® (Atorvastatin 10 mg/kg B.W., Pfizer, USA) by daily gavage. All experiments were approved by the Alfred Medical Research Education Precinct (AMREP) Animal Ethics Committee (E/0998/2010/B).

Tissue processing and histological analysis

Animals were sacrificed using Euthal (10mg/kg, Delvet Limited, Seven Hills, Australia). After blood samples were collected, a catheter was placed in the left ventricle for perfusion with 10 ml PBS, pH 7.4 under physiological pressure. After perfusion, the entire aortic arch with the brachiocephalic artery and the right and left carotid artery was embedded in optimal cutting temperature compound (Sakura Finetechnical), frozen over liquid nitrogen and stored at -20°C until sectioning. 6µm thick longitudinal and transversal cryosections were prepared using a cryostat (Zeiss MICROM HM 550). For longitudinal sections, section angles were adjusted until they revealed a maximum vessel lumen from the brachiocephalic artery to the common carotid artery. Sections were histologically stained with either standard Mayer's hematoxylin/eosin, Oil red O to detect lipids or Picro-sirius Red to detect collagen. Quantification of histological samples for each segment was performed on sequential 6 um sections obtained at 120µm intervals. The percentage of the various plaque components was quantified as the positive area for each specific parameter divided by the total intimal plaque area. The necrotic core was defined as the total plaque area devoid of cellular tissue. Relative cap thickness was defined as the ratio of the cap thickness at the shoulder and mid-plaque region divided by maximal intimal thickness.[1]

Lipid concentrations in mouse serum

Blood samples (0.5-1 ml) were taken by cardiac puncture at the time of sacrifice and placed at room temperature for one hour to clot before being centrifuged at 2000 g for 15 min. Serum was removed and stored at -80°C until analysis. Total serum cholesterol concentrations were measured with a Cobas Integra ® 400 plus Autoanalyzer using the following kits: Cholesterol Gen.2, HDL-Cholesterol plus 2nd generation, LDL-Cholesterol plus 2nd generation, and Triglycerides (Roche Diagnostics, Mannheim, Germany). Colorimetric changes were measured at 512nm for cholesterol and triglycerides or at 583nm for HDL and LDL.

Carotid endarterectomy specimens

Atherosclerotic plaque samples were collected from routinely performed carotid endarterectomies at

the Alfred Hospital and conducted in accordance to ethics approval by the Alfred Hospital Ethics Committee (Project 130/11).

Immunohistochemistry

Frozen sections were thawed and incubated with primary antibodies for one hour at room temperature. The primary antibodies used were anti-CD31 (clone MEC13.3; 1:100 dilution, BD); anti-CD41 (clone MWReg30; 1:100 dilution, Ebioscience); anti-MCP-1 (cat AF479; 1:100 dilution; R&D Systems); anti-ubiquitin (cat U5379; 1:50 dilution; Sigma Aldrich); rabbit anti-mouse fibrin[2] (1:10,000 dilution); anti-MOMA-2 (MCA-519G; 1:100 dilution, Serotec); anti-SMA (clone 1A4; 1:100 dilution. Sigma Aldrich); anti-CD45 (30-F11; 1:50, Ebioscience); anti-CD3 (17A2; 1:50, eBioscience). Detection was achieved by Vectastain ABC kit and DAB substrate. Rat IgG2B control antibodies were used to validate the staining specificity of Rat antibody. Other isotype control antibodies (Goat IgG, rabbit IgG) were used for the validation of each immunostaining according to the primary antibodies. Expression of antigens was quantified using Optimus 6.2 VideoPro-32 and the stained segments were expressed as a percentage of the total plaque area as described previously.[3]

mRNA and miR quantitative polymerase chain reaction (qRT-PCR)

To obtain sufficient quantities of RNA, identical vessel segments from 20 mice were pooled for each sample. Each sample was obtained in triplicate. Overall, 60 ApoE$^{-/-}$ mice on HFD were used 7 weeks after the TS surgical procedure. Total RNA was extracted from freshly isolated vessel segments using 5:1 saturated phenol/chloroform (AMRESCO). After RNA extraction, RNA purity was checked by 260/280 nm ratio. The ratio from each segment was in the range between 1.8 and 2.06, which indicates a high purity RNA extraction. Further confirmation of RNA quality by 1% denaturing agarose gel stained with ethidium bromide, demonstrating clear bands of the 28S and 18S rRNAs. RNA was reverse transcribed into cDNA using TaqMan Reverse Transcription Reagents (Applied Biosystems). To quantify miR, we used the miScript Reverse Transcription kit (Qiagen) follow by miSCript Primer Assays kit (Qiagen). Subsequently, qRT-PCR was conducted using a standard SYBR Green detection on an Applied Biosystem 7500 system (Applied Biosystem). Gene expression was normalized relative to the expression of the housekeeping gene 18S ribosomal RNA using the formula $2^{-\Delta\Delta CT}$.

Illumina gene expression and miR expression analysis

Total RNA isolation was the same as was performed for qRT-PCR. For gene expression, biotin-labeled cRNA was produced by means of a linear amplification kit (AMIL1791; Ambion, Austin, TX) using 250ng of quality checked total RNA as input. Hybridization to the Illumina Mouse WG-6 v2 BeadChip was for 16 hours at 58ºC on a BeadChip Hyb Wheel using 1,500ng biotin-labeled cRNA as input. Afterwards, the chip was washed, blocked and stained with Cy3-streptavidin (Amersham Bioscience) according to manufacturer's protocols (Illumina). Scanning used the iScan Control Software V1.6.20.7 (Illumina) together with the Illumina iSCAN platform (Illumina). Annotation information for the individual chip formats is publicly available from Illumina.

Measurement of miR expression was performed according to Illumina standard protocols for the cDNA-mediated annealing, selection, extension and ligation (DASL) procedure (Illumina). Briefly, 200ng of total RNA was polyadenylated using Poly-A polymerase and converted to cDNA using a biotinylated oligo-dT primer. The cDNA was hybridized to the Illumina Mouse MicroRNA Expression Beadchip (version 2; MI-202-1124) containing probes for 1,146 miR species, extended, ligated and washed according to standard protocols. The beadchips were scanned using the Illumina iScan platform (Illumina).

Processing and analysis of the microarray data were performed with the Illumina Beadstudio 3.1.3.0 software. Raw data were background subtracted and normalized using the "Quantile" algorithm. Quantile normalization assumes that all samples have similar distribution of transcript abundance and make the distribution, median and means of probe intensities the same for every sample. Further analysis was performed in a R-bioconductor environment (Using BRB ArrayTool 4.1.0) and Partek GS 6.10.0915® tool. Images and result lists are shown from Partek, since there was no significant

difference. Selection for differentially expressed genes was performed on the basis of reference to a healthy vessel (vessel segment IV), which did not reveal atherosclerotic plaques, as thresholds for fold changes plus statistical significance according to an Illumina custom model ($p<0.05$) and fold change of greater than 2 or less than 0.5 fold.

Pathway analysis on mRNA and miR expression data was performed using Ingenuity Pathway Analysis (IPA) and GeneGo Inc.. Only annotated genes with a P-value <0.05 and predicted target genes of miR with a fold change greater than 2, or less than 0.5 fold and p-value <0.05 were considered. Target prediction was performed with TargetScan 6.2 and only unique target genes were used for subsequent analysis.

Cell culture and miRNA inhibition

RAW 264.7 macrophages were maintained in Dulbecco's modified medium (Invitrogen) containing 10% FBS (HyClone, South Logan, UT) at 37°C in a 5%CO_2 atmosphere. For inhibition of miR-322, RAW 264.7 macrophages were transfected with anti-miR-322 (miR-322: ACATGAATTGCTGC) and anti-miR-scramble (miR-scramble: ACGTCTATACGCCCA) (Exiqon, meRCURY LNA™) at a final concentration of 50nM using Lipofectamine™, according to manufacturer's instructions (Invitrogen). RAW 264.7 macrophages were stimulated with TNF-α at final concentration 5ng/ml for 4 hours before cells were harvested for RNA extraction. To measure the transfection efficiency, the miR-322 target gene *FGF7* served as a reporter.

Online Tables

Online Table I: Total cholesterol, Triglyceride, HDL, VLDL/LDL in mouse plasma

Parameters	7wks 150µm TS	7wks 450µm TS	Sham	7wks 150µm TS + statin	7wks 150µm SS
Total Cholesterol	32.9 ± 1.7	36.9 ± 4.9	32.2 ± 5.1	40.9 ± 4.0	35.6 ± 6.3
Triglycerides	1.3 ± 0.1	1.7 ± 0.6	1.5 ± 0.6	1.9 ± 0.2	2.0 ± 0.7
HDL	9.8 ± 0.6	10.3 ± 1.3	9.2 ± 0.7	10.9 ± 0.9	10.7 ± 0.1
VLDL/LDL	30.1 ± 2.4	31.4 ± 4.4	28.6 ± 5.1	34.4 ± 3.5	29.5 ± 4.4

Plasma lipid levels in mice subjected to different treatments as depicted.

Data shown as mean ± SEM in mmol/L; n=12 mice per group

Online Table II: List of up- or downregulated miR in vessel segments I & II compared to IV & V ranked by fold change

Probe set ID	Fold Change segment I & II (unstable) vs. segment IV (no plaque) & V (stable)	p-value
mmu-miR-450a-5p	6.43321	1.49E-05
mmu-miR-335-3p	4.8937	0.00221035
mmu-miR-138*	4.30902	3.36E-05
mmu-miR-147	4.02971	1.71E-06
mmu-miR-503*	3.83497	3.10E-05
mmu-miR-322	3.5043	8.73E-05
mmu-miR-351	3.34357	2.03E-06
mmu-miR-298	2.96186	0.000256246
mmu-miR-542-5p	2.95437	6.18E-05
solexa-2011-236**	2.7101	0.0128104
mmu-miR-34c	2.66545	0.00224663
mmu-miR-322*	2.64445	2.00E-05
mmu-miR-503	2.5449	2.40E-06
mmu-miR-296-5p	2.52538	4.02E-05
mmu-miR-15b*	2.39309	4.26E-05
solexa-173-2522**	2.29945	0.00394287
mmu-miR-138	2.23249	0.000879765
mmu-miR-450b-3p	2.22325	6.40E-06
mmu-miR-342-5p	2.17596	0.00060834
mmu-miR-146b	2.11707	9.12E-06
mmu-miR-130b*	2.09015	0.00173715
mmu-miR-142-3p	2.06367	0.00225792
solexa-5306-86**	2.05756	0.00191186
mmu-miR-505	2.03834	0.00554233
mmu-miR-142-5p	2.02477	0.0010853
mmu-miR-499	-2.0976	0.005638
mmu-miR-509-5p	-2.21287	4.58E-07
mmu-miR-669f	-2.23529	0.00203656
solexa-783-586**	-3.17262	0.00399928
mmu-miR-669i	-3.71306	0.0010111

* Complementary sequence

** Solexa Illumina chip array microRNA ID

Online Table III: Ingenuity pathway analysis of dysregulated genes in mRNA expression analysis comparing vessel segments I & II to III, IV & V

Diseases and Disorders

Name	p-value	# Molecules
Inflammatory Response	3.90E-26 - 7.79E-06	148
Cancer	6.79E-16 - 1.23E-05	217
Organismal Injury and Abnormalities	1.08E-15 - 1.03E-05	115
Connective Tissue Disorders	2.43E-15 - 1.03E-05	104
Inflammatory Disease	2.43E-15 - 1.18E-05	109

Molecular and Cellular Functions

Name	p-value	# Molecules
Cellular Movement	5.62E-30 - 1.22E-05	166
Cell-To-Cell Signaling and Interaction	6.07E-20 - 8.89E-06	153
Cellular Growth and Proliferation	2.18E-18 - 9.78E-06	206
Cell Death and Survival	1.95E-17 - 9.43E-06	188
Cellular Development	2.67E-17 - 8.00E-06	181

Physiological System Development and Function

Name	p-value	# Molecules
Hematological System Development and Function	8.40E-30 - 1.22E-05	164
Immune Cell Trafficking	8.40E-30 - 1.22E-05	123
Cardiovascular System Development and Function	2.69E-24 - 1.13E-05	140
Organismal Development	2.69E-24 - 1.13E-05	162
Tissue Morphology	1.51E-21 - 1.13E-05	157

Online Table IV: Ingenuity pathway analysis combining gene expression profiling and target prediction of dysregulated miRs

Diseases and Disorders

Name	p-value	# Molecules
Cancer	8.47E-15 - 1.10E-04	127
Organismal Injury and Abnormalities	1.02E-13 - 1.10E-04	52
Inflammatory Response	8.66E-13 - 1.05E-04	78
Cardiovascular Disease	1.64E-12 - 6.73E-05	63
Dermatological Diseases and Conditions	6.15E-11 - 5.20E-05	27

Molecular and Cellular Functions

Name	p-value	# Molecules
Cellular Movement	5.95E-19 - 1.11E-04	93
Cell Death and Survival	5.89E-15 - 1.10E-04	110
Cellular Growth and Proliferation	1.25E-13 - 9.31E-05	119
Cellular Development	1.63E-11 - 1.07E-04	116
Cellular Function and Maintenance	1.64E-11 - 1.07E-04	98

Physiological System Development and Function

Name	p-value	# Molecules
Cardiovascular System Development and Function	3.63E-18 - 8.15E-05	82
Organismal Development	3.63E-18 - 8.06E-05	103
Immune Cell Trafficking	4.44E-13 - 1.10E-04	62
Organismal Survival	1.68E-12 - 2.80E-09	71
Hematological System Development and Function	4.63E-12 - 1.07E-04	90

Online Table V: List of upregulated genes (>5-fold) in vessel segments I & II in comparison to vessel segments III, IV, and V

Gene Symbol	Fold Changes Absolute	p-value
Prl2c2	18.15	0.0093
Prl2c3	14.28	0.0036
Il1b	10.95	0.0032
LOC100048710	10.90	0.0021
Hmox1	10.61	0.0036
Clec4n	10.13	0.0048
Slc40a1	9.85	0.0038
Prl2c4	9.57	0.0042
Irg1	8.22	0.0092
Kit	8.17	0.0039
Adamts4	7.97	0.0073
Esm1	7.91	0.0026
Pcdh12	7.53	0.0026
Adamts7	7.46	0.0024
Upp1	7.21	0.0055
Upp1	7.10	0.0049
Hdc	7.02	0.0049
Sirpb1	6.59	0.0090
Rgs16	6.42	0.0046
Fpr2	6.11	0.0026
LOC100046802	5.78	0.0076
Ifitm1	5.74	0.0049
Mmp9	5.65	0.0070
Wisp1	5.54	0.0013
Egln3	5.49	0.0026
Bmper	5.48	0.0043
S100a9	5.46	0.0089
Retnlg	5.09	0.0075

Online Figures and Figure legends

Online Figure I

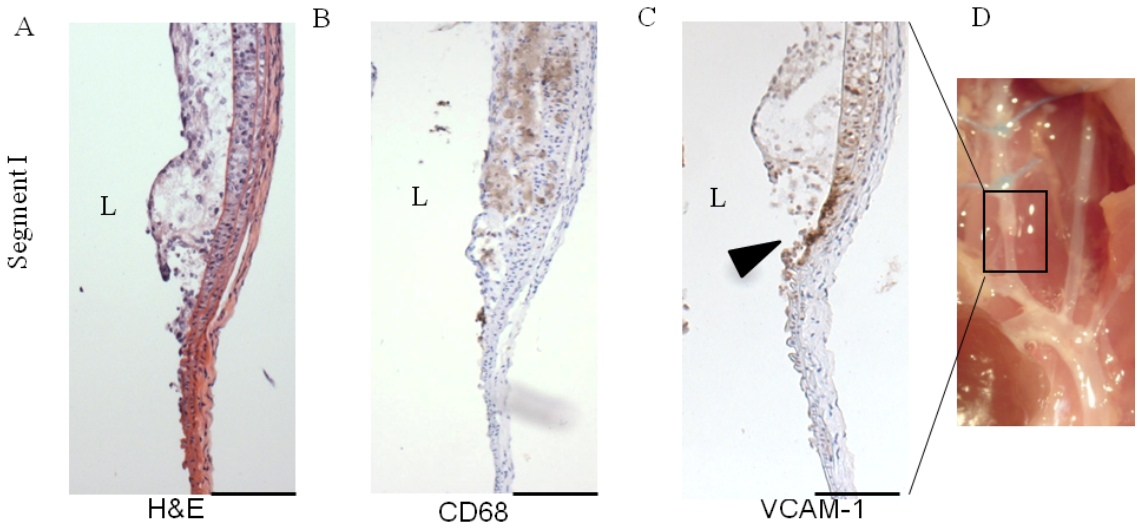

Online Figure I: Gross anatomy and longitudinal histology of segment I two weeks after TS surgery. (**A**) H&E staining demonstrates atherosclerotic plaque development. The free lumen is labeled with L. (**B**) Immunostaining of CD68 revealed a strong accumulation of macrophages/foam cells in vessel segment I. (**C**) Immunostaining of VCAM-1 represents strong inflammatory reactions (arrow head). (**D**) Macroscopic picture of the discussed vessel segments with the blue sutures visible at the areas of the two stenoses. No luminal thrombosis or IH can be found at this time point. Bars indicate 200µm.

Online Figure II

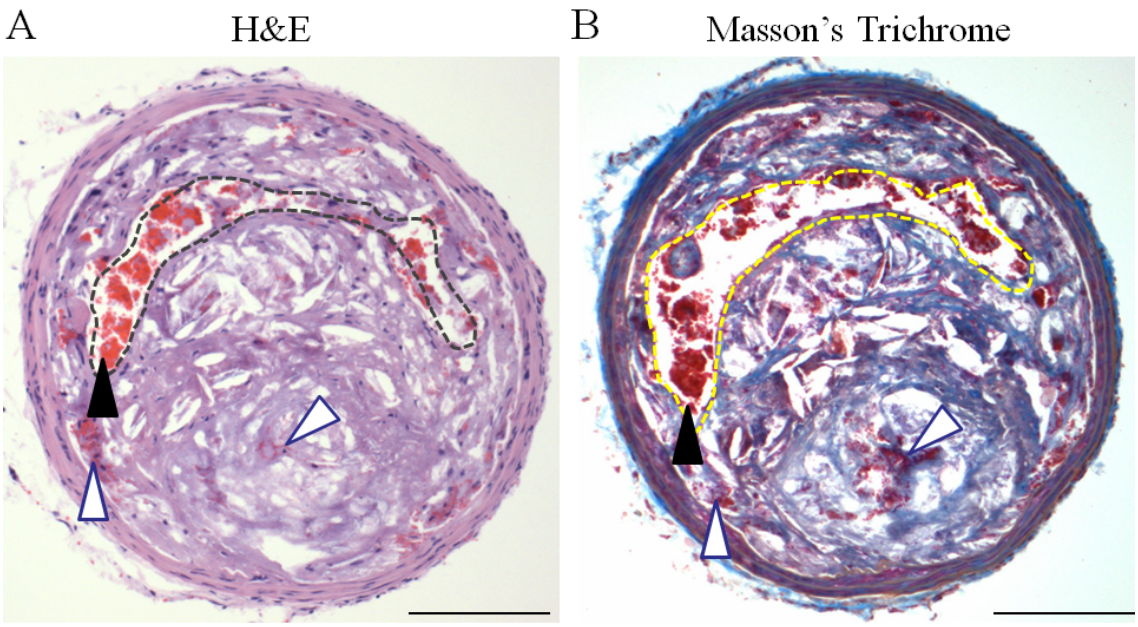

Online Figure II: **Histological examples of unstable atherosclerotic plaques from vessel segment I 11 weeks after TS surgery.** H&E (**A**) and Trichrome staining (**B**) depict intraplaque hemorrhage (IH; white arrow heads), which is often associated with intraluminal hemorrhage (black arrow heads). Large cholesterol crystals can be seen. The dashed lines encircle the vessel lumen. RBCs present in bright red in H&E and dark red in trichrome staining. Bars indicate 250μm.

Online Figure III

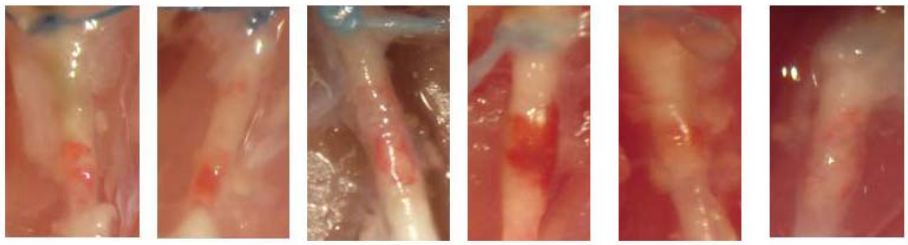

Online Figure III: Examples of macroscopically visible intraplaque hemorrhages (IH) upstream (proximal) of the proximal stenosis (vessel segment I) in the TS mouse model at 7 weeks after surgery. Photos were taken with a 10x dissecting microscope. The proximal blue sutures are visible.

Online Figure IV

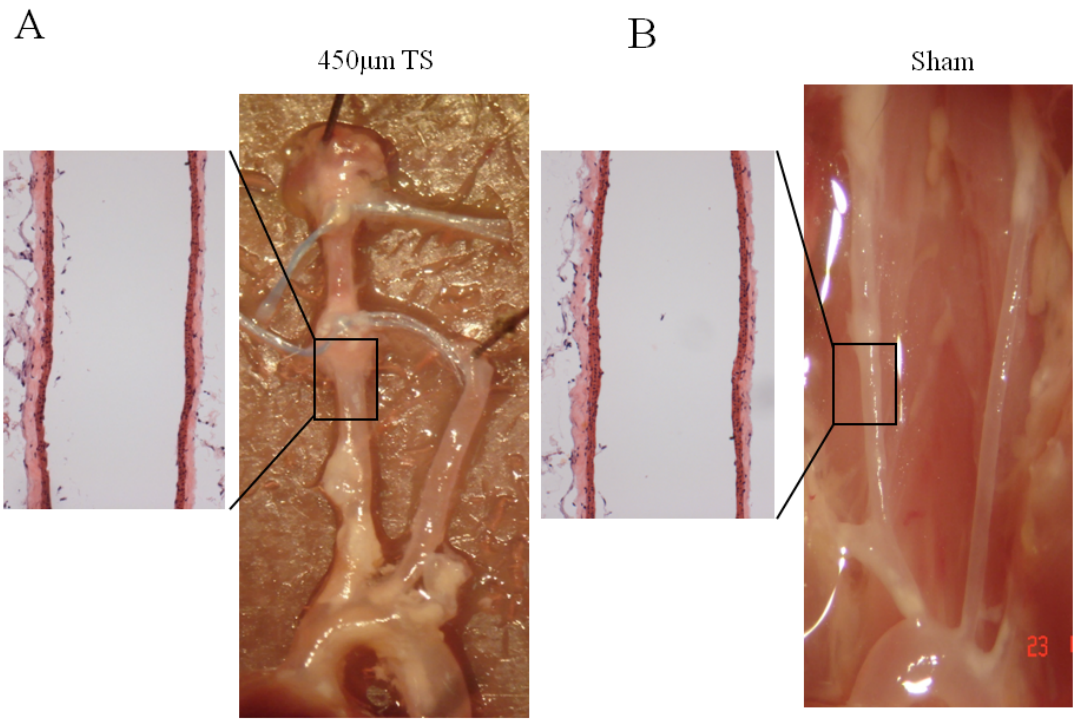

Online Figure IV: Controls for the TS model: (A) non-constrictive stenosis (450µm) and (B) sham operated mice. Gross anatomy and H&E staining of longitudinally sectioned vessel at 11 weeks after surgery demonstrate that the sutures and the operation on their own do not induce the atherosclerotic plaque build-up or intraplaque hemorrhage as seen in the TS (150µm) surgery model.

Online Figure V

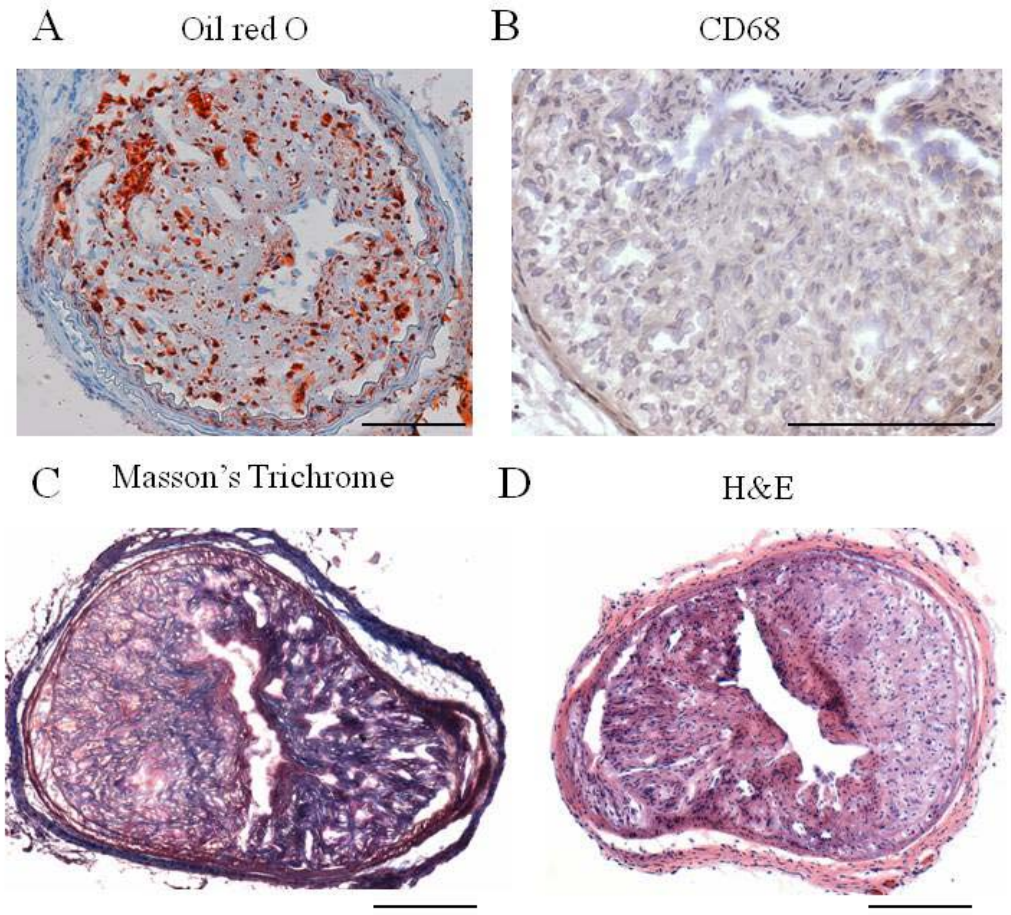

Online Figure V: Histological characterization of atherosclerotic plaques in mice with total ligation of the right carotid artery for 7 weeks. (**A**) Low levels of lipid content (Oil Red O) and (**B**) low abundance of $CD68^{+}$ macrophages were observed in the total ligation model. (**C**) Atherosclerotic plaques displayed strong collagen staining and extensive neointimal hyperplasia. (**D**) H&E staining reveals that total ligation did not induce the development of necrotic cores or formation of fibrous caps. Bars indicate 250μm.

Online Figure VI

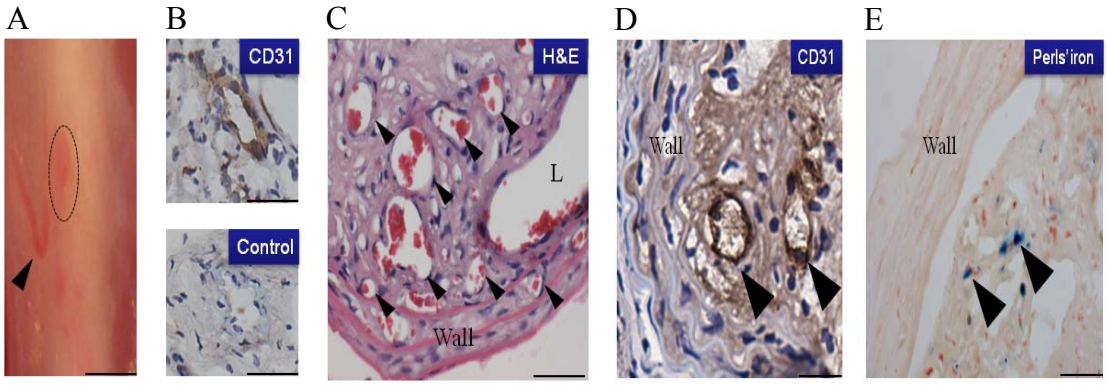

Online Figure VI: ***Neo vasa vasora*** **as typical features of plaque instability in segment I of the TS mouse model.** (**A**) *Neo vasa vasora* in the adventitia were visible macroscopically (arrow indicates a new vessel adjacent to IH, which is depicted by a dotted circle). (**B**) Staining of adventitia with anti-CD31 antibody also indicates a newly formed vessel. (**C**) Intraplaque microvessels could be found adjacent to the original lumen (arrows indicate intraplaque microvessels). (**D**) Notably, newly formed vessels with single layers of endothelial CD31-positive cells and Perls' iron staining (**E**) were often found adjacent, which indicates the presence of old hemorrhage. L: Lumen. Bars indicate 500μm in A and 50μm in B, C, D, and E. C is stained with H&E.

Online Figure VII

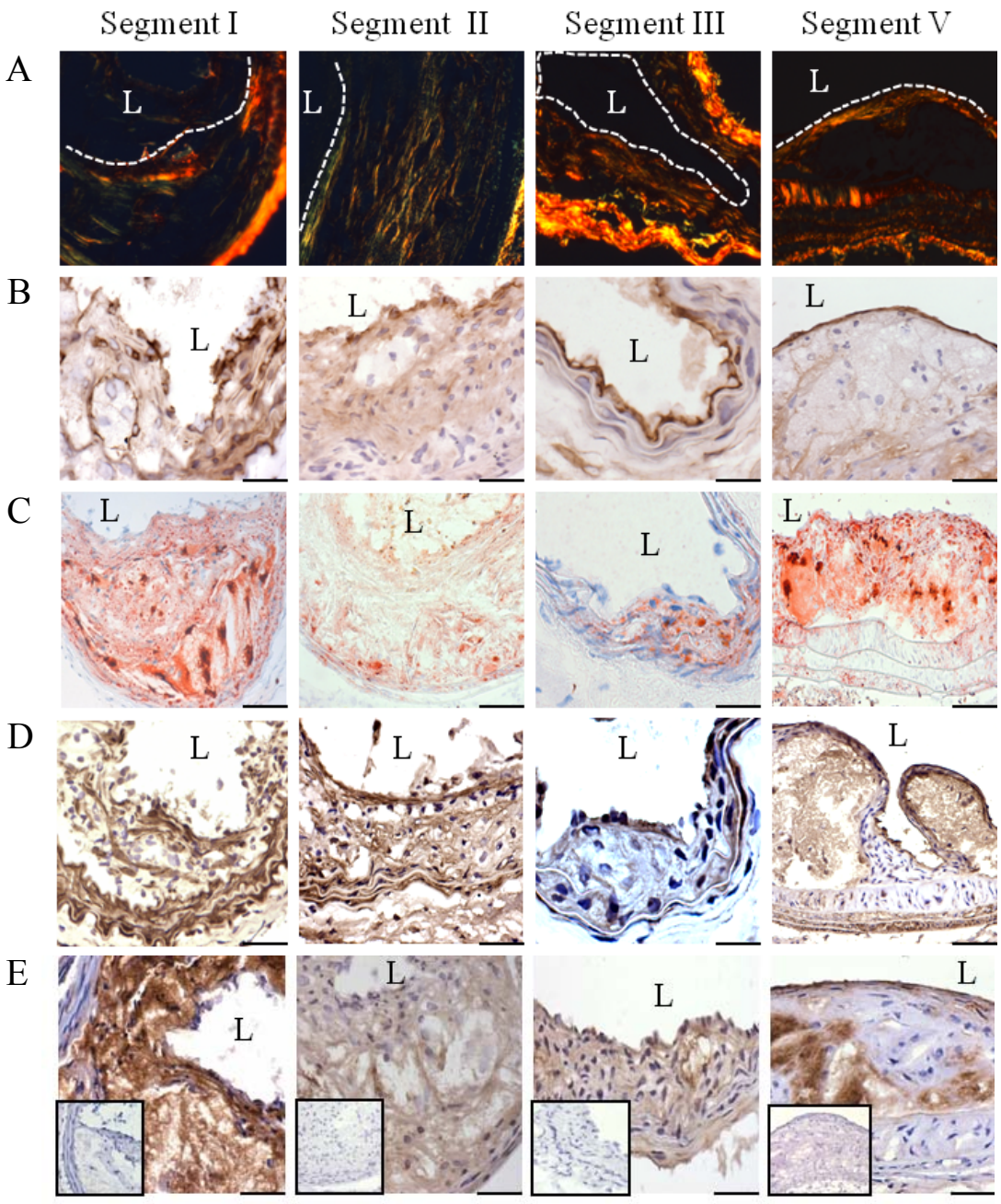

Online Figure VII: Histological analysis of the TS model 7 weeks after surgery. Representative staining of (**A**) collagen (Picro-Sirius Red), (**B**) CD31, (**C**) lipid (Oil Red O), (**D**) SMCs (anti-SMC α-actin), (**E**) MOMA-2 (Isotype control in the insert) in segment I, II, III and V. L: Lumen. Bars indicate 50μm.

Online Figure VIII

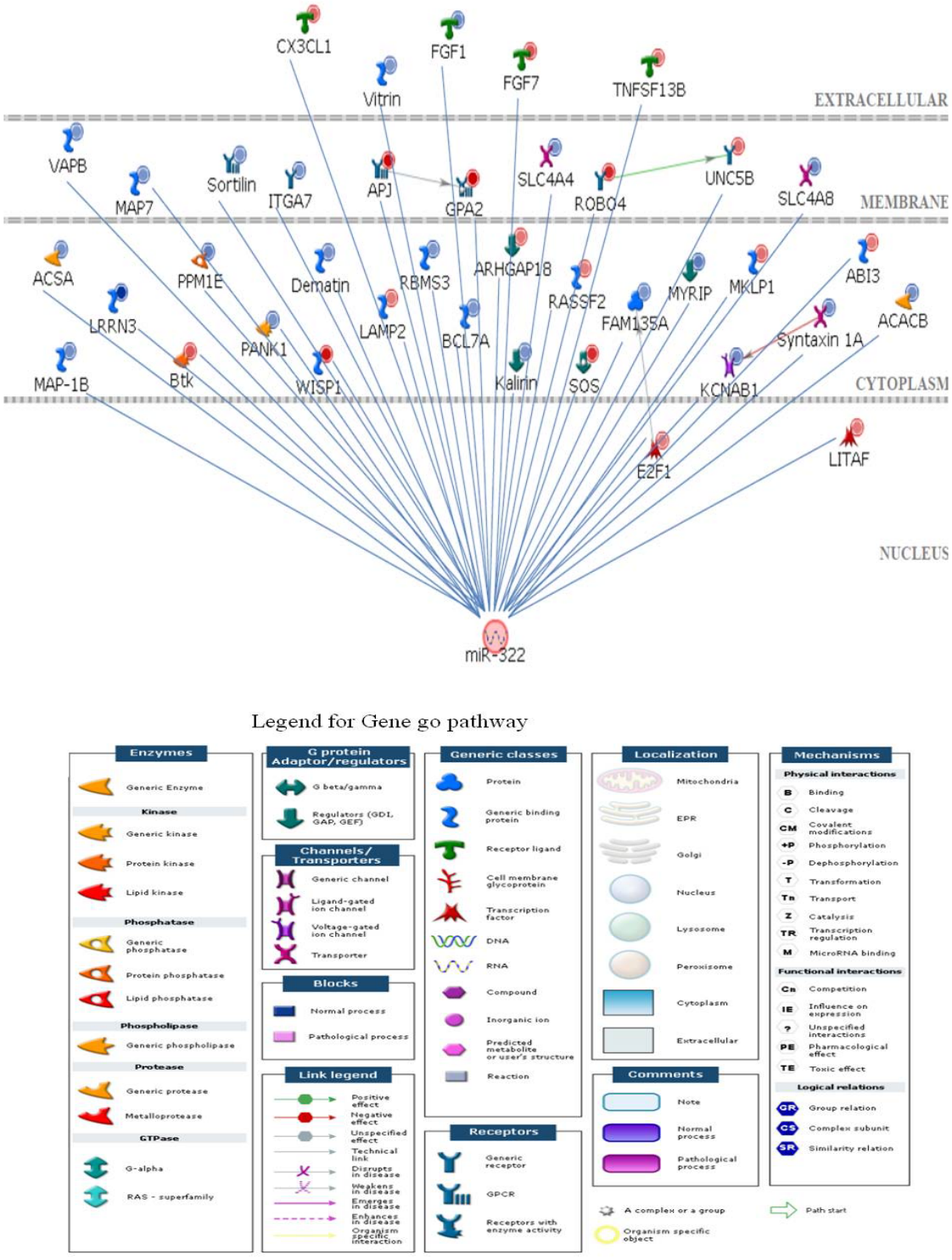

Online Figure VIII: Network map of experimentally validated miR-322 target genes differentially expressed in unstable (segment I) and stable (segment V) atherosclerotic plaques. Upregulated genes are marked with red circles. Downregulated genes are marked with blue circles. The network map was generated using GeneGo.

Online Figure IX

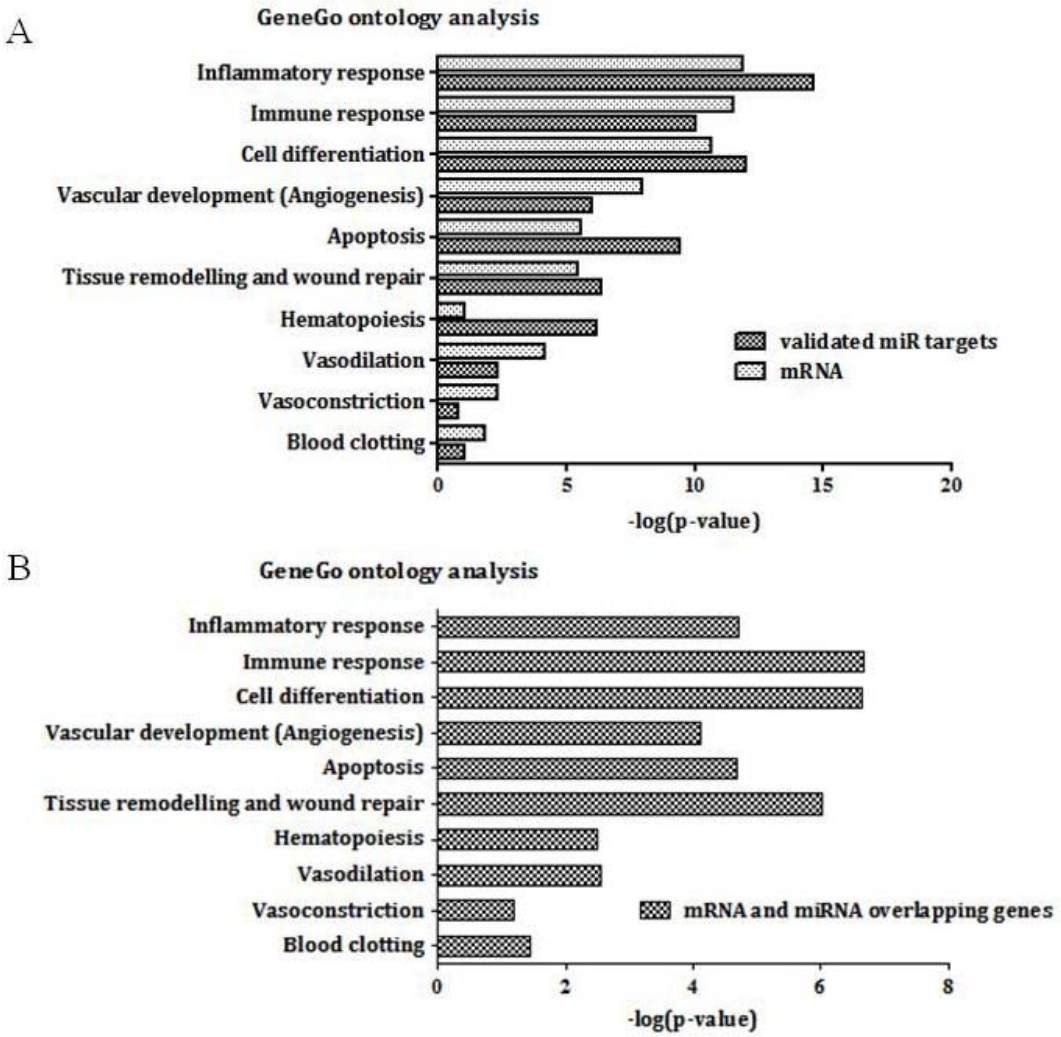

Online Figure IX: GeneGo pathway analysis of combined mRNA and miR data sets. (**A**) Main gene ontologies of differentially expressed genes and validated miR target genes. (**B**) Main gene ontologies of differentially expressed genes overlapping with predicted and validated miR target genes.

Online Figure X

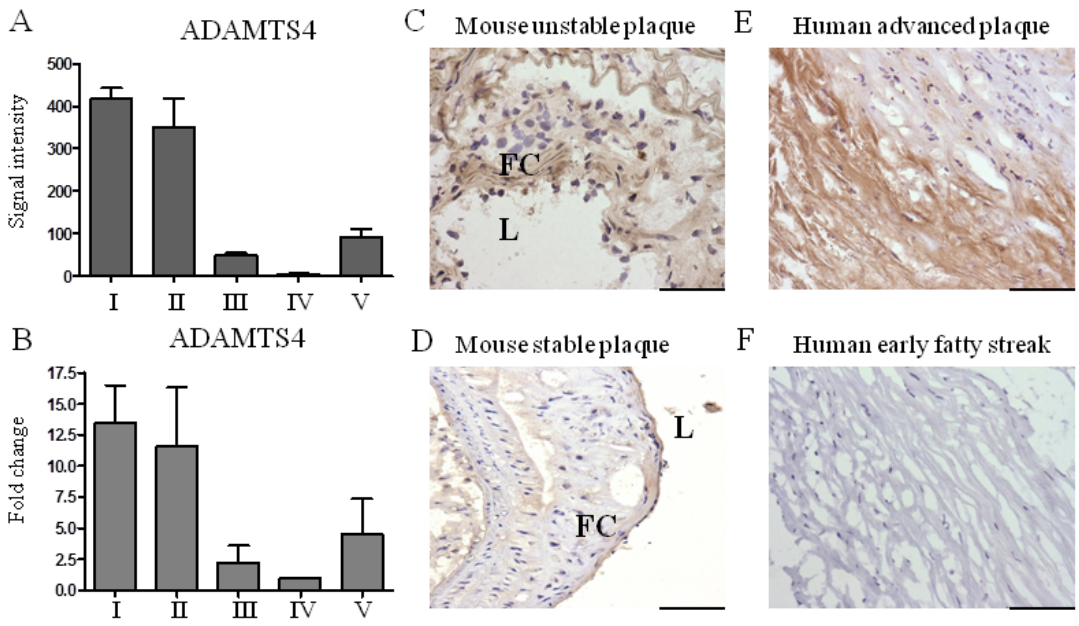

Online Figure X: ADAMTS4 is highly expressed in murine unstable plaques and human carotid advanced plaque. (**A**) Signal intensity from microarray data demonstrates a significant upregulation of ADAMTS4 in vessel segment I (unstable plaque) compared to segment V (stable plaque). (**B**) Similarly, using qRT-PCR, a significant upregulation of ADAMTS4 was found in segment I compare to segment V. (**C**) Immunohistochemistry shows high expression of ADAMTS4 in fibrous caps of segment I of unstable atherosclerotic plaques of mice. (**D**) Low expression of ADAMTS4 was detected in segment V (stable plaques in mouse aortic arch). In human atherosclerotic plaques obtained by carotid endarterectomy, ADAMTS4 is highly abundant in advanced lesion (**E**) but not in early fatty streak lesion (n=8). (**F**). All numerical data are given as mean ± SEM. Bars indicate 50µm in C and D, and 100µm in E and F. All data are depicted as mean ± SEM, normalised to 18s and expressed as fold change relative to segment IV (healthy vessel).

Online References

1. Cheng C, Tempel D, Den Dekker WK, Haasdijk R, Chrifi I, Bos FL, Wagtmans K, van de Kamp EH, Blonden L, Biessen EA, Moll F, Pasterkamp G, Serruys PW, Schulte-Merker S, Duckers HJ. Ets2 determines the inflammatory state of endothelial cells in advanced atherosclerotic lesions. *Circ Res*. 2011;109:382-395.
2. Drew AF, Tucker HL, Liu H, Witte DP, Degen JL, Tipping PG. Crescentic glomerulonephritis is diminished in fibrinogen-deficient mice. *Am J Physiol Renal Physiol*. 2001;281:F1157-1163.
3. To K, Agrotis A, Besra G, Bobik A, Toh BH. Nkt cell subsets mediate differential proatherogenic effects in apoe-/- mice. *Arterioscler Thromb Vasc Biol*. 2009;29:671-677.